skb.se

SKB P-23-01

ISSN 1651-4416
ID 2000279
March 2023
Updated 2023-05

HM-COMSOL status report 2022

Ola Kristensson
Clay Technology

Keywords: Continuum mechanics, Material model, Bentonite, Comsol Multiphysics

This report concerns a study which was conducted for Svensk Kärnbränslehantering AB (SKB). The conclusions and viewpoints presented in the report are those of the author. SKB may draw modified conclusions, based on additional literature sources and/or expert opinions.

Data in SKB's database can be changed for different reasons. Minor changes in SKB's database will not necessarily result in a revised report. Data revisions may also be presented as supplements, available at www.skb.se.

This report is published on www.skb.se

The original report, dated March 2023, was found to contain editorial errors which have been corrected in this updated version.

Abstract

The Hysteresis Based Material (HBM) model is here described. The report is an attempt to give a full description of the formulation and the implementation in COMSOL Multiphysics®. Some parts of the model are discussed in greater detail; mass balances, total stress, clay potential functions, evolution equations governing the path dependent variable, and micro void ratio evolution equation. To facilitate future corrections and development, full derivations of a significant part of the model are included in the appendices. The goal has been to give a clear and transparent description where entities are defined when introduced and assumptions are declared.

Sammanfattning

Här beskrivs den HysteresBaserade Materialmodellen (HBM). Rapporten är avsedd att ge en fullständig beskrivning av formuleringen och implementationen i COMSOL Multiphysics®. Några delar av modellen är beskrivna i detalj; massbalanser, totalspänning, lerpotentialfunktioner, evolutionsekvationerna av den vägberoende variabeln och evolutionsekvationen för mikroportalet. För att underlätta framtida korrektioner och utveckling så är härledningar för stora delar av formuleringen inkluderat i appendix. Målet har varit att ge en klar och transparent beskrivning där storheter definieras när de introduceras och antaganden är tydligt deklarerade.

Contents

1 Introduction

This report describes the formulation of the Hysteresis Based Material (HBM) model of compacted bentonite which has been developed within the project "Hydromechanical modelling using COMSOL Multiphysiscs®". The description follows the formulation as it stands at the end of 2022. Information about the implementation of the HBM-model in COMSOL Multiphysiscs® is also given.

It should from the start be pointed out that this report is of theoretical character. No specific problems are set up and solved. The report is intended to describe the general formulation without specifying geometries, parameter values, etc.

If information about the capabilities and performance of the model when solving specific problems is sought, this can be found in reports produced within work package 3 and 5 of the EU-funded Bentonite Mechanical Evolution (BEACON) project, see Gens (2018, 2020, 2021), Talandier (2019, 2020a, 2020b), Charlier et al. (2021), and Talandier et al. (2022). It should, however, be noted that the version of HBM presented in this report has not been used within BEACON. The main difference is the described evolution equation for the path dependent variable, which was developed and implemented after the end date of BEACON.

The new version has, however, been used within Task 13 of the Task Force on Engineered Barrier Systems (EBS TF). This was also the first time that wall friction and HBM were successfully solved together in a simulation. The simulation could however not be calculated in its entirety. Friction is often part of the problem formulations which SKB want to address, for example along the deposition hole wall and the tunnel wall. Contact and friction mechanics are well known for being numerically demanding and when combined with other nonlinear representations the complexity often results in numerical simulations which do not converge. During this project there have been several attempts to solve problems where both friction and HBM were included, but it is only the most recent which has shown progress. The ability to use HBM and friction in the same model indicates that the usability of the formulation has improved with the latest modification of the path dependent variable.

The project started in 2016, in part because of difficulties when carrying out simulations of homogenization tasks within the EBS TF, see Börgesson et al. (2020) and Dueck et al. (2019). It had, however, for a long time been known that the available material models had limitations which made a new model desirable. The project was aimed at developing a model for bentonite where the fundamental driving forces are a starting point rather than an afterthought. An equally important part was developing an implementation which can be used for simulating realistic conditions and geometries. The work has been carried out in parallel with the BEACON project, which provided suitable tasks where the new model could be tested and demanded new features being developed and implemented.

Thus, HBM was developed in part due to needs identified while carrying out large amounts of thermo-hydro-mechanical (THM) simulations of bentonite components in different environments. The available material models at that time could be used successfully but were found to have limited capabilities. For example, they had difficulties in representing essential material characteristics such as the swelling pressure curve, behaviour during free swelling, and the strong coupling between hydraulics and mechanics. To obtain representative results, the parameter setup often demanded a prediction of the processes which were to take place in the simulation. Also, the range for which the models were accurate, was quite narrow. Thus, the allowed heterogeneity in the simulations was restricted.

The short introduction to the basis of HBM given below should serve as a good starting point for what follows in the report. In section 2 a full but brief description of the model is given. More information about the formulation can be found in section 3 where the balance equations and mechanical material model are discussed in more detail. The implementation into COMSOL Multiphysics® is described in section 4, where the treatment of mass balances and mechanics are discussed separately. In section 5, final comments and conclusions are given. For completeness, to facilitate understanding, as well as for facilitating future development, there are appendices containing information about the formulation on several topics: Appendix A. Theoretical framework, Appendix B. Solid mass balance, Appendix C. Balance of water mass, Appendix D. Spherical/deviatoric-split, Appendix E. Stiffness components at shearing and constant suction,

Appendix F. Rate form of the stress relation, and Appendix G. Strain-driven formulation of the limiting condition of $\boldsymbol{f}$.

1.1 Introduction to the HBM formulation

Here, a short introduction and overview of the mechanical material model within HBM is given to provide a good starting point for the more detailed information in the rest of the report. To facilitate understanding, it begins with describing an isotropic and saturated version of the model, the generalization to handling of general stress states and unsaturated states are then included at the end.

At the core of HBM constitutive relations, the difference between chemical potentials μ_c and μ_0, belonging to the water within a saturated clay sample and its external water respectively, is coupled to the pressure, p, acting on the clay. The constitutive relation comes from expressing the chemical potential of the water within the saturated clay sample when it is pressurized,

$$\mu_c = \mu_0 + RT\ln\frac{p_c}{p_0} + \nu p\,, \tag{1-1}$$

where R is the universal gas constant, T absolute temperature, p_c the vapor pressure measured above the clay sample, p_0 the vapor pressure measured above the external water, and ν the molar volume of water. The fraction in vapor pressure defines relative humidity, $RH = p_c/p_0$. (1-1) can be rearranged to,

$$p + s = \Psi\,, \tag{1-2}$$

where the suction, s, and a clay potential, Ψ, have been defined according to,

$$s = -\frac{\mu_c - \mu_0}{\nu}, \qquad \text{and} \quad \Psi = -\frac{RT}{\nu}\ln(RH)\,, \tag{1-3}$$

respectively. The clay potential can be linked to both hydraulic and mechanical experimental results such as swelling pressure, deviator stress at failure, retention at wetting, and retention at drying. The character of mechanical and retention experimental data indicate that the bentonite clay potential should be dependent on dry density, ρ_d, and incorporate hysteresis, i.e., path dependency.

To incorporate this, the clay potential is made dependent on the void ratio, $e = \rho_s\backslash\rho_d - 1$ (ρ_s being the solid density), and a path dependent variable, f, is introduced, i.e., $\Psi = \bar{\Psi}(e, f)$. The path dependency comes from an evolution equation of f,

$$f = f_0 + \int_{e_0}^{e(t)} \frac{\partial f}{\partial e}\,de\,, \tag{1-4}$$

which, in this isotropic model, is driven by void ratio. The differential in (1-4) is made dependent on the magnitude of f and direction changes (history) of e. Figure 1-1 shows an example of how a cyclic void ratio history gives a path dependence in f and Ψ. The incorporation of the path dependence (hysteresis) is why the model was called the hysteresis-based material model.

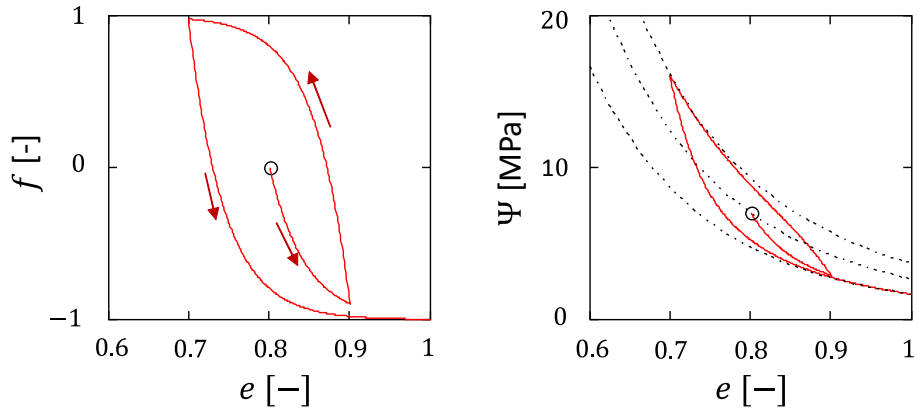

Figure 1-1. Path dependent variable, $\boldsymbol{f}$, and clay potential, $\boldsymbol{\Psi}$, versus void ratio, $\boldsymbol{e}$. The left graph shows an example of the path variable for a cycle of swelling-consolidation-swelling. The right graph shows the response for the clay potential for the same cycle.

The model discussed so far is isotropic, generalizing to general stress states gives the expression,

$$s\mathbf{1} = \boldsymbol{\Psi} + \boldsymbol{\sigma}^{\mathrm{I}}\,, \tag{1-5}$$

where a stress tensor for the saturated clay, $\boldsymbol{\sigma}^{\mathrm{I}}$, and clay potential tensor, $\boldsymbol{\Psi}$, has been introduced. In this formulation the path dependent variable is a tensor, $\boldsymbol{f}$, which is dependent on the strain evolution.

The above is valid for the saturated clay phase, i.e., mineral sheets and interlayer water. When generalizing to unsaturated states, a gas phase is introduced. Thus, the unsaturated clay can be viewed as an immiscible mixture of a saturated clay phase and a gas phase. The additional pore space makes it possible to distinguish between interlayer pore space and total pore space. A total void ratio can be obtained from, $e = \rho_s \backslash \rho_d - 1$, and a micro void ratio can be obtained from, $e_\mu = w\rho_s \backslash \rho_w$, where w is the gravimetric water content and ρ_w the water density.

When introducing gas pores in the material it can be thought of as the volume and outer surface area of a representative volume element (RVE) increases. The stresses present in the saturated clay phase, $\boldsymbol{\sigma}^{\mathrm{I}}$, must somehow be reduced as to translate these to a total stress, $\boldsymbol{\sigma}$, representative for the entire RVE. This was done by introducing a contact area variable α, approximating the ratio of the contact area between saturated clay grains to total area of an RVE so that,

$$\boldsymbol{\sigma} = \alpha\boldsymbol{\sigma}^{I}\,. \tag{1-6}$$

2 Brief description of HBM

This chapter contains a brief description of the HBM model. The description of the model starts with the adopted material structure from which definitions of quantities enable formulation of balance equations. Thereafter constitutive equations of the liquid phase, gas phase and the mechanics of the porous solid are described. More information can be found in chapter 3, Appendix A, Appendix B, and Appendix C.

The energy balance has not been addressed here. If vapor diffusion is to be represented this would be needed. In the present description however, isothermal conditions are assumed.

2.1 Material structure assumptions

In Figure 2-1 a sketch of the assumed material structure is given to the left and a descriptive diagram to the right. The adopted clay material structure can be described using a tree diagram which visualize the hierarchical nature of the model. The top-level, or macro-level, is populated by the clay which can be saturated or unsaturated. The clay is an immiscible mixture of two phases populating the mid-level, or meso-level. The first phase on the meso-level is saturated clay grains and the second gas filled pores. The phase consisting of saturated clay grains is an immiscible mixture of two phases populating the lower-level, or micro-level. The phase of gas filled pores is a miscible mixture of dry air and water vapor. The two phases at the micro-level, the building blocks of the phase of saturated clay grains, are interlayer water and minerals.

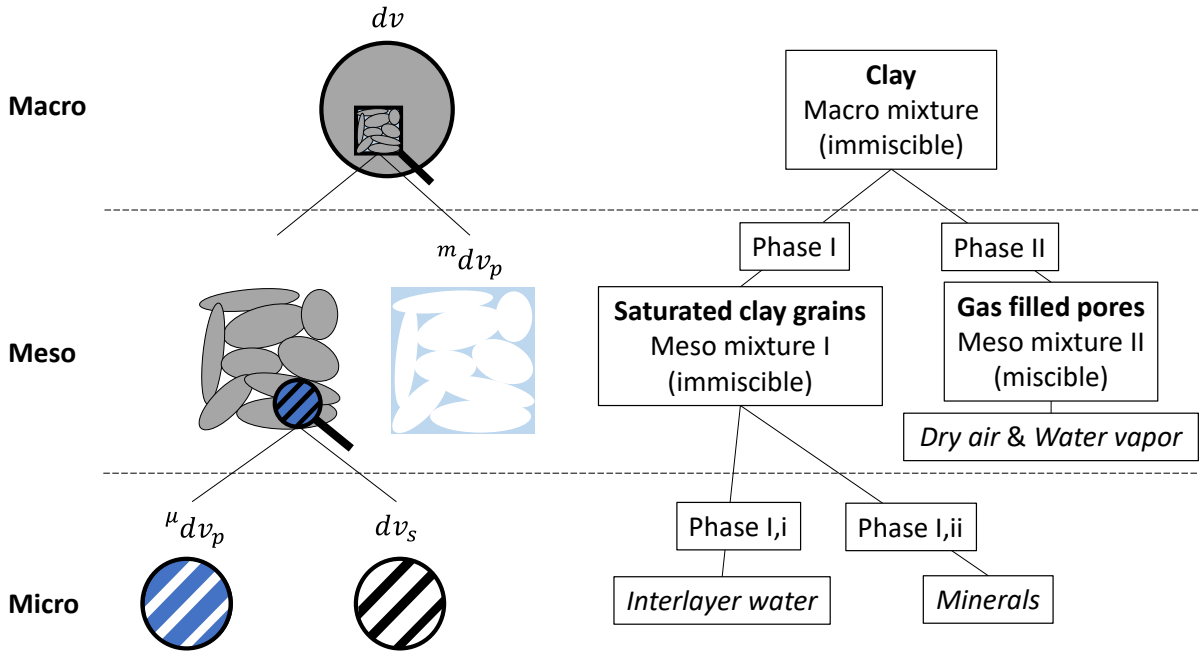

Figure 2-1. Description of the adopted material structure.

To the left in Figure 2-1, volume elements needed for the formulation are identified. From using these, different void ratios can be formulated. The total void ratio is defined by,

$$e = \frac{dv_p}{dv - dv_p} = \frac{^{\mu}dv_p + {}^{m}dv_p}{dv - (^{\mu}dv_p + {}^{m}dv_p)}. \tag{2-1}$$

The total porosity is given by,

$$\phi = \frac{dv_p}{dv} = \frac{^{\mu}dv_p + {}^{m}dv_p}{dv} = \frac{e}{1+e}. \tag{2-2}$$

The immiscibility of phases at the micro-level makes it possible to define a micro void ratio,

$$e_\mu = \frac{{}^{\mu}dv_p}{dv_s}. \tag{2-3}$$

When discussing the total stress at unsaturated states in section 3.2.1 a meso porosity, ϕ_m, is used. It is defined as,

$$\phi_m = \frac{{}^{m}dv_p}{dv} = 1 - \frac{1+e_\mu}{1+e} \tag{2-4}$$

and is, as shown, possible to express in terms of total and micro void ratios.

As indicated in the right diagram of Figure 2-1, and in the first paragraph of this section, volumes in the structure are allotted specific constituents (mineral, water and air):

- The meso pore space contains dry air and water vapor: ${}^{m}dm_p = dm_g{}^{a} + dm_g{}^{w}$
- The micro pore space contains interlayer water: ${}^{\mu}dm_p = dm_l{}^{w}$
- The solid volume contains minerals: $dm_s = dm_m$

The above gives that $dv_g = {}^{m}dv_p$, $dv_l{}^{w} = {}^{\mu}dv_p$ and that there is a solid volume element dv_s. The degree of liquid saturation can then be expressed as,

$$S_l = \frac{dv_l{}^{w}}{dv_p} = \frac{e_\mu}{e}. \tag{2-5}$$

Using mass elements and volume elements makes it possible to formulate mass densities:

$$\rho_s = \frac{dm_s}{dv_s}\,, \rho_l = \frac{dm_l{}^{w}}{dv_l{}^{w}} \text{ and } \rho_g = \frac{dm_g{}^{a}}{dv_g} + \frac{dm_g{}^{w}}{dv_g} = \theta_g{}^{a} + \theta_g{}^{w}\,. \tag{2-6}$$

2.2 Balance equations

Using what is defined above, balance equations of solid mass, water mass and force can be formulated.

The solid mass balance,

$$\dot{e} = (1+e)\,\dot{\varepsilon}_v\,, \tag{2-7}$$

is expressed in terms of total void ratio and the volumetric strain invariant $\varepsilon_v = \mathrm{tr}\boldsymbol{\varepsilon}$, where the small strain tensor, $\boldsymbol{\varepsilon} = 0.5(\mathrm{Grad}\boldsymbol{u} + (\mathrm{Grad}\boldsymbol{u})^T)$, is defined by displacement gradients, $\mathrm{Grad}\boldsymbol{u}$.

The water mass balance,

$$\begin{aligned}\dot{\rho}_l e_\mu(1-\phi) + \rho_l \dot{e}_\mu(1-\phi) + \mathrm{div}(\rho_l \boldsymbol{v}^{d,l}) + \dot{\theta}_g{}^{w}\big(e-e_\mu\big)(1-\phi) + \theta_g{}^{w}\dot{e}(1-\phi) \\ - \theta_g{}^{w}\dot{e}_\mu(1-\phi) + \mathrm{div}\big(\theta_g{}^{w}\boldsymbol{v}^{d,g}\big) = f\end{aligned} \tag{2-8}$$

is expressed in terms of total porosity, total and micro void ratio, liquid water density, vapor mass per gas phase, liquid water mass flux $\rho_l \boldsymbol{v}^{d,l}$, and vapor mass flux $\theta_g{}^{w}\boldsymbol{v}^{d,g}$. The liquid Darcy flux, $\boldsymbol{v}^{d,l}$, and gas Darcy flux, $\boldsymbol{v}^{d,g}$, are defined as,

$$\boldsymbol{v}^{d,l} = e_\mu(1-\phi)(\boldsymbol{v}^l - \boldsymbol{v})\,, \text{and } \boldsymbol{v}^{d,g} = \big(e-e_\mu\big)(1-\phi)(\boldsymbol{v}^g - \boldsymbol{v})\,. \tag{2-9}$$

The force balance,

$$\mathrm{div}\boldsymbol{\sigma} + \boldsymbol{b} = \boldsymbol{0}\,, \tag{2-10}$$

is expressed in terms of the stress tensor, $\boldsymbol{\sigma}$, and the body force, $\boldsymbol{b}$.

2.3 Constitutive equations

The chosen independent variables, for which the balance equations are solved for, is the set consisting of displacements, $\boldsymbol{u}$, and suction, s. The latter is related to the difference in chemical

potential between the interlayer water of the clay and a chosen referential state (normally that of the groundwater), see (1-3). If the thermal problem is to be solved, the energy balance and temperature, T, will be added to the equation system and independent variables, respectively. Below, however, only isothermal conditions are considered.

To complete the formulation, material specific relations are specified for the remaining variables. If not stated, pressures are given in Pa and temperatures in K in the equations below. An assumption of a uniform gas pore pressure field, where $p_g = 0.1$ MPa, has been used. A tilde above a character indicate that it is a function and the same character without a tilde indicates a parameter given by that function, i.e., $a = \tilde{a}(x)$.

The interlayer water is specified by the liquid density,

$$\tilde{\rho}_l(s) = {\rho_l}^0 \exp(-\alpha s)\,, \tag{2-11}$$

with reference value ${\rho_l}^0$ and a compressibility α, and the Darcy flux,

$$\boldsymbol{v}^{d,l} = \tilde{\boldsymbol{q}}_l(e, e_\mu, s) = \frac{\tilde{\kappa}(e, e_\mu)}{\mu}\mathrm{grad}s\,, \tag{2-12}$$

driven by gradients in suction. μ denotes the viscosity and $\tilde{\kappa}(e, e_\mu)$ the permeability function given by,

$$\tilde{\kappa}(e, e_\mu) = \kappa_0 \left(\frac{e}{e_{ref}}\right)^{\beta} \left(\frac{e_\mu}{e}\right)^{\lambda}, \tag{2-13}$$

where κ_0 and e_{ref} are reference values, β determines the dependence on void ratio, and λ the dependence on degree of water saturation. As shown earlier, see (2-5), the fraction formed by micro void ratio and total void ratio is equal to the degree of water saturation.

The gas phase is assumed to be a mixture of two ideal gases, water vapor and dry air. Thus, $p_g = {p_g}^w + {p_g}^a$, where ${p_g}^w$ and ${p_g}^a$ denote the partial gas pressures for the water and air constituents, respectively. The formulation agrees with that of CODE_BRIGHT. The gas density, ρ_g, can be expressed in terms of the two constituents' "relative" densities, vapor mass per gas phase, ${\theta_g}^w$, and dry air mass per gas phase, ${\theta_g}^a$, see (2-6),

$$\tilde{\rho}_g(s,T) = \tilde{\theta}_g{}^w(s,T) + \tilde{\theta}_g{}^a(s,T)\,. \tag{2-14}$$

The constituents' relative densities are given by,

$$\tilde{\theta}_g{}^w(s,T) = \frac{M_w}{RT}\,\tilde{p}_g{}^w{}_{sat}(T)\widetilde{RH}(s,T), \tag{2-15}$$

$$\tilde{\theta}_g{}^a(s,T) = \frac{M_a}{RT}\left(p_g - \tilde{p}_g{}^w{}_{sat}(T)\widetilde{RH}(s,T)\right), \tag{2-16}$$

where

$$\tilde{p}_g{}^w{}_{sat}(T) = 136075 \cdot 10^6 \exp\left(\frac{-5239.7}{T}\right), \tag{2-17}$$

$$\widetilde{RH}(s,T) = \exp\left(\frac{-sM_w}{RT{\rho_l}^0}\right). \tag{2-18}$$

In the expressions above $M_w = 0.018$ mol/kg, $M_a = 0.029$ mol/kg and $R = 8.314472$ J/mol/K. The vapor diffusion flux $\boldsymbol{i}_g{}^w$ is driven by a gradient in vapor mass concentration grad$c$,

$${}^m\theta_g{}^w\boldsymbol{v}^{d,g} = \boldsymbol{i}_g{}^w = -\tilde{\boldsymbol{D}}(e, e_\mu, s, T)\mathrm{grad}c\,. \tag{2-19}$$

$\tilde{\boldsymbol{D}}(e, e_\mu, s, T)$, the diffusion coefficient function, is given by,

$$\tilde{\boldsymbol{D}}(e, e_\mu, s, T) = \tau\phi\tilde{\rho}_g(s,T)\left(1 - \frac{e_\mu}{e}\right) D\,\frac{T^{2.3}}{p_g}\mathbf{1}\,, \tag{2-20}$$

where τ denotes the tortuosity, ϕ the porosity, and D the diffusion coefficient of vapor. Since the vapor mass concentration can be formulated using the expressions for the densities ${\theta_g}^w$ and ρ_g,

$$\tilde{c}(s,T) = \left[\frac{\tilde{\theta}_g{}^w(s,T)}{\tilde{\rho}_g(s,T)}\right], \tag{2-21}$$

the gradient can be expressed in terms of gradients in suction and temperature,

$$\mathrm{grad}c = \frac{\partial \tilde{c}(s,T)}{\partial s}\mathrm{grad}s + \frac{\partial \tilde{c}(s,T)}{\partial T}\mathrm{grad}T\,. \tag{2-22}$$

As mentioned above, the present description has not included the energy balance and only isothermal conditions are considered, the temperature gradient in the expression above is therefore zero.

The mechanical material model relates stress to deformation (strain) and suction. The total stress $\boldsymbol{\sigma}$ for unsaturated/saturated states is given by scaling the saturated grain stress $\boldsymbol{\sigma}^{\mathrm{I}}$ by a contact area variable α,

$$\boldsymbol{\sigma} = \alpha\boldsymbol{\sigma}^{I}\,. \tag{2-23}$$

The contact area variable approximates the ratio of the contact area between saturated grains to total area of a representative volume element. The contact area variable is given by the function,

$$\alpha = \tilde{\alpha}\left(e, e_\mu\right) = \left(\frac{1+e_\mu}{1+e}\right)^{\gamma}, \tag{2-24}$$

where γ defines the shape of the function. It is worth to note that the bracketed expression is equal to the volume fraction of the clay phase which can be expressed $1-\phi_m$, using the meso porosity defined in (2-4).

As discussed in chapter 1, the thermodynamically motivated relation of HBM, describing the hydromechanical coupling for a saturated system can be expressed,

$$-\boldsymbol{\sigma}^{I} = \boldsymbol{\Psi} - s\mathbf{1}\,. \tag{2-25}$$

The stress in the saturated grains is here related to suction and a quantity which is called clay potential tensor, $\boldsymbol{\Psi}$. Thus, the clay potential tensor can be viewed to bridge the mechanical and hydraulic processes.

Experimentally determined retention and swelling pressures for bentonite show a dependency on void ratio and the path which the state has been arrived at. The clay potential is therefore made dependent on void ratio and a path dependent variable $\boldsymbol{f}$, according to,

$$\boldsymbol{\Psi} = \widetilde{\Psi}_M\left(e_\mu\right)\mathbf{1} + \widetilde{\Psi}_\Delta\left(e_\mu\right)\boldsymbol{f}\,. \tag{2-26}$$

The present formulation uses two functions dependent on the micro void ratio, $\widetilde{\Psi}_M\left(e_\mu\right)$ and $\widetilde{\Psi}_\Delta\left(e_\mu\right)$. The first one being a "mean" function and the second a "deviation" function multiplied to the path dependent variable.

The path dependent variable is governed by a limiting condition and an evolution equation driven by strain, given by,

$$F = R^2 - \left({f_p}^2 + {f_q}^2\right) \tag{2-27}$$

$$\frac{\partial \boldsymbol{f}}{\partial \boldsymbol{\varepsilon}} = \begin{cases} -\boldsymbol{K}\dfrac{F}{R^2} & dF < 0 \\ -\boldsymbol{K} & dF \geq 0 \end{cases}, \qquad \boldsymbol{K} = K_{ijkl}\boldsymbol{e}_i \otimes \boldsymbol{e}_j \otimes \boldsymbol{e}_k \otimes \boldsymbol{e}_l\,, \tag{2-28}$$

where the invariants f_p and f_q are obtained from,

$$f_p \equiv \frac{1}{3}\mathrm{tr}\boldsymbol{f} \quad \text{and} \quad {f_q}^2 \equiv \frac{3}{2}\boldsymbol{f}^{dev}\cdot\boldsymbol{f}^{dev}\,, \tag{2-29}$$

where,

$$\boldsymbol{f}^{dev} = \boldsymbol{f} - f_p\,\mathbf{1}. \tag{2-30}$$

The final part of the mechanical constitutive relations is an evolution equation of the micro void ratio,

$$de_\mu = \frac{\partial e_\mu}{\partial e} de + \frac{\partial e_\mu}{\partial s} ds\,, \tag{2-31}$$

The first of the differentials describes a kinematical coupling to the total void ratio and the second describe the swelling of the saturated clay grains at the micro scale given a change in suction. The first differential is chosen as being given by the contact area function,

$$\frac{\partial e_\mu}{\partial e} = \tilde{\alpha}(e, e_\mu), \tag{2-32}$$

and the second differential by,

$$\frac{\partial e_\mu}{\partial s} = \begin{cases} \dfrac{(e - e_\mu)\widetilde{\Psi}_M(e_\mu)}{s} \dfrac{1}{(e - e_\mu)\dfrac{\partial \widetilde{\Psi}_M}{\partial e_\mu} - \widetilde{\Psi}_M(e_\mu)} & \text{if } \dot{s} < 0 \\ \dfrac{-e_{step}}{\left|s - \widetilde{\Psi}_M(e_\mu - e_{step})\right|} & \text{otherwise} \end{cases}. \tag{2-33}$$

3 Additional information about HBM

This chapter contains additional/complementary information about the HBM formulation to what was given in the brief description in chapter 2. More information about the derivations/descriptions in this chapter can be found in the referenced appendices and Larsson (2012).

In 3.1 some steps in the derivation of the mass balance equations and the final results are given. Detailed derivations of the mass balances can be found in Appendix B and Appendix C. The solid mass balance and the connection to a proper updating-scheme for the void ratio/porosity and a clear definition of the Darcy-flow (in terms of velocities and pore structure variables) are described.

In 3.2 the mechanical constitutive relations are discussed in more detail. Studies of the connections between the homogenized stress approach and the present formulation might give new insights about how to view some of the used mechanical entities and how to proceed forward. The clay-potential plays a central role in the model and its connection to experiments is described next. The most recent part of the formulation, the new relations governing the rate dependent variable, are given together with a graphical representation. The relations governing the micro void ratio are also described.

3.1 Mass balance equations

3.1.1 Solid mass balance

The solid mass per mixture volume can be expressed,

$$\frac{dm_s}{dv} = \frac{dm_s}{dv_s}\frac{dv_s}{dv} = \rho_s(1-\phi). \tag{3-1}$$

The total solid mass $\mathcal{M}^s$ is obtained from integrating the expression above over the body,

$$\mathcal{M}^s = \int_{\mathcal{B}} \rho_s(1-\phi)dv \ . \tag{3-2}$$

Taking the time derivative with respect to the solids reference configuration gives the global form of the solid mass balance,

$$\frac{D^s\mathcal{M}^s}{Dt} = \dot{\mathcal{M}}^s = 0 \, . \tag{3-3}$$

Using (3-3) a local form of the solid mass balance can be derived. From this, the following three relations for updating the void ratio, using the volumetric strain, can be derived. Note that only the first relation updates the void ratio without approximations.

$$\dot{e} = (1+e)\dot{\varepsilon}_v, \qquad e \approx (1+e_0)(\varepsilon_v+1)-1, \qquad \text{and} \quad \dot{e} \approx (1+e_0)\dot{\varepsilon}_v \tag{3-4}$$

3.1.2 Liquid water mass balance

The liquid water mass per mixture volume can be expressed as,

$$\frac{dm_l{}^w}{dv} = \frac{dm_l{}^w}{dv_l{}^w}\frac{dv_l{}^w}{dv_s}\frac{dv_s}{dv} = \rho_l e_\mu(1-\phi) \tag{3-5}$$

The total liquid water mass $\mathcal{M}^l$ is obtained from,

$$\mathcal{M}^l = \int_{\mathcal{B}} \rho_l e_\mu(1-\phi)dv \tag{3-6}$$

After taking the time derivative and performing several steps, the local form of the balance of liquid water mass reads,

$$\dot{\rho}_l e_\mu(1-\phi) + \rho_l \dot{e}_\mu(1-\phi) + \mathrm{div}(\rho_l \boldsymbol{v}^{d,l}) = f_l{}^w \, . \tag{3-7}$$

Here $f_l{}^w$ is a source term and $\boldsymbol{v}^{d,l}$ the Darcian velocity, defined by $\boldsymbol{v}^{d,l} = e_\mu(1-\phi)\boldsymbol{v}^{r,l}$, where the relative velocity $\boldsymbol{v}^{r,l} = \boldsymbol{v}^l - \boldsymbol{v}$, between the liquid phase and solid phase is introduced.

3.1.3 Gaseous water mass balance

The gaseous water mass per mixture volume can be expressed as,

$$\frac{dm_g{}^w}{dv} = \frac{dm_g{}^w}{dv_g}\frac{dv_g}{dv_s}\frac{dv_s}{dv} = \theta_g{}^w\big(e - e_\mu\big)(1-\phi) \tag{3-8}$$

The total gaseous water mass $\mathcal{M}^g$ is obtained from,

$$\mathcal{M}^g = \int_{\mathcal{B}} \theta_g{}^w\big(e - e_\mu\big)(1-\phi)dv. \tag{3-9}$$

Performing the same procedure as for the liquid phase the local form of the balance of gaseous water is obtained as,

$$\dot{\theta}_g{}^w\big(e - e_\mu\big)(1-\phi) + \theta_g{}^w\dot{e}(1-\phi) - \theta_g{}^w\dot{e}_\mu(1-\phi) + \mathrm{div}\big(\theta_g{}^w\boldsymbol{v}^{d,g}\big) = f_g{}^w\,, \tag{3-10}$$

where $f_g{}^w$ is a source term, and $\boldsymbol{v}^{d,g} = \big(e - e_\mu\big)(1-\phi)\boldsymbol{v}^{r,g}$ the Darcian velocity expressed in terms of the relative velocity $\boldsymbol{v}^{r,g} = \boldsymbol{v}^g - \boldsymbol{v}$ between the gas phase and solid phase.

3.2 Mechanical material model

The basis of the total stress used in HBM is discussed in 3.2.1, the clay potential functions in chapter 3.2.2, the path dependent variable in chapter 3.2.3, and the micro void ratio evolution equation in chapter 3.2.4.

3.2.1 Total stress in HBM and total stress in a homogenized stress framework

As described in (2-23), in HBM the total stress is given by scaling a saturated grain stress by a contact area variable, approximating the ratio between the contact area between saturated grains and the total area for a representative volume element (RVE). In this section the relation between the HBM formulation and that used in a homogenized stress framework is investigated. Homogenized stress is commonly part of formulations representing mixtures.

First, some basic context is given, and the general theory of the homogenized stress is outlined. The next step is to express the unsaturated clay system at the meso-level, where it contains the two phases: (I) saturated clay and (II) gas, within the homogenized framework, see Figure 2-1. Thereafter follows a comparison between HBM and the homogenized formulation. Finally, the mechanics taking place at the scale of individual clay grains are discussed to find out if what was found when comparing the formulations seems reasonable.

Below, two "scales" will be denoted by microscopic and macroscopic, respectively. They should not be confused with the macro, meso, and micro, used when describing the different levels in the material structure assumptions. All entities (variables and parameters) in HBM belong to what below is denoted the macroscopic scale, i.e., we use a macroscopic representation of the material. This is mentioned since the nomenclature could be somewhat confusing. For instance, the micro void ratio e_μ is a macroscopic variable which contains information about the material at the microscopic level. Both notations, for the material structure levels and scales in the homogenized stress framework, serve their purposes, and better ones have not yet been found.

In the homogenized stress formulation, the total stress of the mixture, $\boldsymbol{\sigma}$, is defined as the volumetric mean value of a "micro stress field", $\boldsymbol{\sigma}_{micro}$, which may vary over an RVE, with volume V. Thus,

$$\boldsymbol{\sigma} = \frac{1}{V}\int_{\mathcal{B}} \boldsymbol{\sigma}_{micro}dv\,. \tag{3-11}$$

The link between the macroscopic and microscopic scale is visible in the definition above. Fields varying over the RVE are microscopic. Fields that are constant over the RVE are macroscopic. The latter statement is also called "the principle of scale separation", which will be used later. One can also say that the RVE is representing a macroscopic point.

If defining a homogenized stress for a mixture where there are several phases, P, their individual contribution to the total stress can be expressed as a summation of phase stresses at the micro-, $\boldsymbol{\sigma}^P{}_{micro}$, and macro-level, $\boldsymbol{\sigma}^P$,

$$\boldsymbol{\sigma} = \frac{1}{V}\sum_{\forall P}\int_{\mathcal{B}^P}\boldsymbol{\sigma}^P{}_{micro}\,dv = \sum_{\forall P}\boldsymbol{\sigma}^P. \tag{3-12}$$

The last equality was obtained by using the principle of scale separation. The homogenized phase stress $\boldsymbol{\sigma}^P$, also denoted *partial stress* of P, can be expressed in terms of an *intrinsic stress* of P, $\boldsymbol{\sigma}^P{}_{in}$, using a volume fraction for the phase, $n^P = V^P/V$,

$$\boldsymbol{\sigma}^P = n^P\boldsymbol{\sigma}^P{}_{in}\,, \tag{3-13}$$

where,

$$\boldsymbol{\sigma}^P{}_{in} = \frac{1}{V^P}\int_{\mathcal{B}^P}\boldsymbol{\sigma}^P{}_{micro}\,dv\,. \tag{3-14}$$

The total stress may thus be expressed as,

$$\boldsymbol{\sigma} = \sum_{\forall P} n^P\boldsymbol{\sigma}^P{}_{in}\,. \tag{3-15}$$

The unsaturated clay is now expressed in the homogenized stress framework. The present model has two phases at the intermediate (meso) level, the saturated clay phase, *I*, and the gas phase, *II*, see Figure 2-1. The volume fraction of phase *II* can be identified as the meso-porosity, see Equation (2-4), $n^{II} = \phi_m = {}^m dv_p/dv$, which gives that, $n^I = 1 - \phi_m$. The intrinsic stress for the second phase is given by the gas pressure, $\boldsymbol{\sigma}^{II}{}_{in} = -p_g\mathbf{1}$. Using this results in,

$$\boldsymbol{\sigma} = (1-\phi_m)\boldsymbol{\sigma}^I{}_{in} - \phi_m p_g\mathbf{1}\,. \tag{3-16}$$

In the HBM-formulation, given by (2-23), (2-24) and (2-4), the macroscopic total stress reads,

$$\boldsymbol{\sigma}^* = (1-\phi_m)^\gamma\boldsymbol{\sigma}^{I*}\,, \tag{3-17}$$

where $\gamma > 1$. The superscript * is used for differentiation between stresses in our formulation from those defined in the homogenized stress formulation. Note that $\boldsymbol{\sigma}^{I*}$ is defined as the stress at fully saturated conditions given by $\boldsymbol{\sigma}^{I*} = -\boldsymbol{\Psi} + s\mathbf{1}$.

To facilitate a comparison between the formulations above, the listing in Table 3-1 is given.

Table 3-1 Type of formulation and stress contributions.

	Stress contributions	
	Phase I: Saturated clay	Phase II: Gas
Homogenized formulation	$(1-\phi_m)\boldsymbol{\sigma}^I{}_{in}$ (a)	$-\phi_m p_g\mathbf{1}$
HBM formulation	$(1-\phi_m)^\gamma\boldsymbol{\sigma}^{I*}$ (b)	

a) $\boldsymbol{\sigma}^I{}_{in} = \frac{1}{V^I}\int_{\mathcal{B}^I}\boldsymbol{\sigma}^I{}_{micro}\,dv$

b) $\boldsymbol{\sigma}^{I*} = -\boldsymbol{\Psi} + s\mathbf{1}$

The listing in Table 3-1 shows that the gas phase pressure contribution has been approximated to zero in HBM,

$$p_g \approx 0\,, \tag{3-18}$$

and when studying the saturated clay stress contributions, the HBM formulation can be viewed as to approximate the intrinsic stress (volume average of micro stress over *I*) by,

$$\boldsymbol{\sigma}^I{}_{in} = \frac{1}{V^I}\int_{\mathcal{B}^I} \boldsymbol{\sigma}^I{}_{micro}\, dv \approx (1-\phi_m)^{\gamma-1}\boldsymbol{\sigma}^{I*}\,. \tag{3-19}$$

In the relation above $\boldsymbol{\sigma}^{I*}$ is scaled by the factor $(1-\phi_m)^{\gamma-1}$, where an exponent $\gamma - 1 > 0$ have been used for representing bentonite, thus, $0 < (1-\phi_m)^{\gamma-1} \leq 1$. HBM may be viewed as approximating the intrinsic stress by reducing the stress at full saturation, $\boldsymbol{\sigma}^{I*}$, by a function increasing with increasing saturation, see Figure 3-1. This can be thought of as if the stress is being transferred more effectively with increasing saturation.

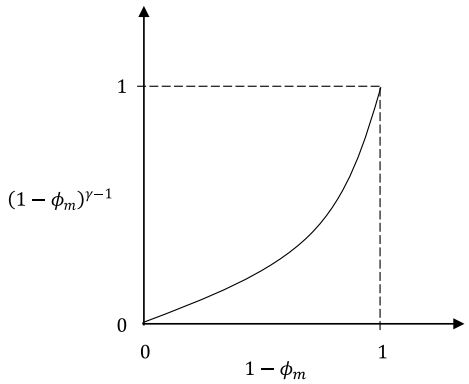

Figure 3-1. Illustration of a typical appearance of the function $(\mathbf{1}-\boldsymbol{\phi_m})^{\boldsymbol{\gamma-1}}$ scaling the stress at full saturation in HBM. $\mathbf{1}-\boldsymbol{\phi_m}$ is equal to the volume ratio of the saturated clay phase.

In the final paragraphs of this section an "evaluation" of the result from the comparison is attempted. For this purpose, the mechanics at the scale of individual clay grains is discussed using a toy model. The given description should only be taken as a rough sketch, focused as to give information necessary for the evaluation: how do the averaged micro stress field depends on the degree of saturation.

The drawing in Figure 3-2 is a schematic illustration of the idea behind the mechanics at the scale of individual clay grains. In the drawing, a saturated grain of clay is illustrated at two states of different water saturation of the mixture. This means that there are different volume ratios of the gas phase in the mixture at the two states, i.e., the meso-porosity, ϕ_m, is different.

At its boundary, the saturated clay grain either faces other saturated clay grains, indicated by (1) or porosities containing the gas phase indicated by (2). In this example it is assumed that the gas pressure is unsignificant as compared to the stress at the grain interfaces. When the grain takes up water it is assumed to swell isotropically. Due to differences in "mechanical support" at (1) and (2) a heterogeneous stress field will develop within the clay grain.

Compressive stresses of higher magnitude will develop between the clay grain interfaces indicated by (1), where there is strong support. In the drawings volumes with high compressive stresses are indicated with hatched boundaries and the symbol + internally. At the interfaces against the gas phase, indicated by (2), there is weak support, the clay swells into the gas filled pores, and normal stresses are unchanged.

When the saturation increases (going from the left to the right drawing) the swelling increases the area of the clay grain interfaces and the area of the gas phase interfaces decreases. The clay grain thereby experiences an increased support from the neighbouring clay grains and the part of the grain which can transfer stresses increases as well. At full saturation (not shown in the drawing) only grain to grain contacts exist and the stress is transmitted perfectly.

Following the reasoning above: the higher the saturation the closer the volume average of the micro stress field is to the higher stress level in the grain. Relation (3-19), found when comparing HBM with the homogenized view, agrees with this reasoning. This indicates that the chosen expression for the area fraction function in HBM agrees well with characters sought in a function for an intrinsic stress in a homogenized formulation.

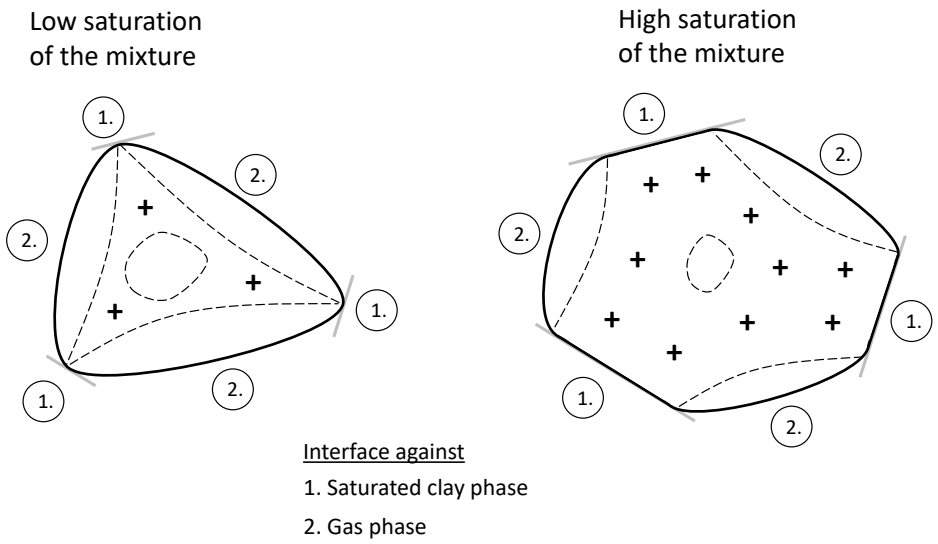

Figure 3-2. Schematic illustration of individual clay grains at two different saturations.

3.2.2 Clay potential functions

When carrying out the modelling tasks in the BEACON project it became obvious that the parametrization and fit of the clay potential function was an essential part in achieving solutions that provide a good representation of experimental behaviour of bentonite. Models which simulate unsaturated conditions require a clay potential with a very good fit to experimental data over a large interval in void ratio. This is due to the large active range in micro void ratio during such simulations, especially so when starting out from very dry conditions (or if the material undergo significant drying).

The clay potential bridges the mechanical and hydraulic processes at the core of the model. A well-designed clay potential function should therefore enable the model to produce both characteristic mechanical and characteristic hydraulic behaviour. This must be kept in mind when selecting the experimental data for calibrating the clay potential, when selecting a suitable parametrization, and performing the fitting. To establish a link from experimental data to the clay potential, several characteristic quantities are defined. These are the swelling pressure, p_s, the deviator stress at failure, q_f, the wetting retention, s_w, and the drying retention, s_d. The clay potential curves, Ψ_M and Ψ_Δ, are then identified in terms of these characteristic quantities. The identification is facilitated by dividing the mechanical model in a spherical and deviatoric part, this is described in Appendix D.

For the mechanical regime, the swelling pressure, p_s, is defined as the minimum pressure attained at full saturation and when suction is zero, and the deviator stress at failure, q_f, (also at full saturation) is defined as the maximum attainable deviator stress,

$$p_s \equiv \min(p) \text{ when } s = 0\,, \tag{3-20}$$

$$q_f \equiv \max(q)\,. \tag{3-21}$$

With these definitions the clay potential contributions Ψ_M and Ψ_Δ can be identified as,

$$\Psi_M = p_s + q_f \text{ and } \Psi_\Delta = \frac{1}{R} q_f\,. \tag{3-22}$$

For the hydraulic regime, the wetting retention, s_w, is defined as the minimum suction obtained under unconfined conditions, and the drying retention, s_d, is defined as the maximum suction obtained under unconfined conditions,

$$s_w \equiv \min(s) \text{ when } \boldsymbol{\sigma} = \mathbf{0}\,, \tag{3-23}$$

$$s_d \equiv \max(s) \text{ when } \boldsymbol{\sigma} = \mathbf{0}\,. \tag{3-24}$$

With the given definitions the clay potential contributions Ψ_M and Ψ_Δ can be identified as,

$$\Psi_M = \frac{s_d + s_w}{2} \text{ and } \Psi_\Delta = \frac{s_d - s_w}{2R}. \tag{3-25}$$

Thus, to achieve proper representations in both regimes (mechanical and hydraulic) both data sets $\{p_s, q_f\}$ and $\{s_d, s_w\}$ must be considered and these must be well suited and consistent when fitting Ψ_M and Ψ_Δ.

3.2.3 Path dependent variable

The history dependency of $\boldsymbol{f}$ is seen in its incremental updating scheme which can be expressed as,

$$\boldsymbol{f} = \boldsymbol{f}_0 + \int_{t_0}^{t} d\boldsymbol{f}\,. \tag{3-26}$$

The increment in the path dependent variable, $d\boldsymbol{f}$, is given by an incremental relation expressed in terms of strain,

$$d\boldsymbol{f} = \frac{\partial \boldsymbol{f}}{\partial \boldsymbol{\varepsilon}} d\boldsymbol{\varepsilon}\,, \tag{3-27}$$

where the partial derivative is a fourth order tensor which can be expressed as,

$$\frac{\partial \boldsymbol{f}}{\partial \boldsymbol{\varepsilon}} = \frac{\partial f_{ij}}{\partial \varepsilon_{kl}} \boldsymbol{e}_i \otimes \boldsymbol{e}_j \otimes \boldsymbol{e}_k \otimes \boldsymbol{e}_l\,. \tag{3-28}$$

The partial derivative is given by,

$$\frac{\partial \boldsymbol{f}}{\partial \boldsymbol{\varepsilon}} = \begin{cases} -\boldsymbol{K}\dfrac{F}{R^2} & dF < 0 \\ -\boldsymbol{K} & dF \geq 0 \end{cases}, \tag{3-29}$$

where $\boldsymbol{K} = K_{ijkl}\boldsymbol{e}_i \otimes \boldsymbol{e}_j \otimes \boldsymbol{e}_k \otimes \boldsymbol{e}_l$ is an unitless "stiffness tensor" and F is part of the limiting condition,

$$F = R^2 - \left({f_p}^2 + {f_q}^2\right), \tag{3-30}$$

where R is a parameter determining the limiting value and the definitions of f_p and f_q are given in (2-29) and (2-30).

In the present model $K_{ijkl} \neq 0$ for components where $i = k$ & $j = l$. Due to symmetry in stress ($\sigma_{ij} = \sigma_{ji}$) we have that $\boldsymbol{f}$ is symmetric and therefore $K_{ijkl} = K_{jikl}$. Symmetry in strain gives that $K_{ijkl} = K_{ijlk}$. The modulus K_{ijkl} governs how "fast" $\boldsymbol{f}$ goes towards the limiting value and have two different values, $K_{ijkl} = K_{aa}$ for the compressive/tensile components such as df_{11}, and $K_{ijkl} = K_{ab}$ for the shear components such as df_{12}. K_{aa} is obtained by fitting the solution of the model against strain-deviator stress evolutions in triaxial tests. K_{ab} was calculated by expressing a given strain state in two different coordinate systems. This resulted in a tensile/compressive representation and a shear representation from which the ratio $K_{ab}/K_{aa} = 1/2$ could be obtained, see Appendix E.

The vector,

$$\boldsymbol{\varphi} \equiv f_p \boldsymbol{e}_p + f_q \boldsymbol{e}_q\,, \tag{3-31}$$

is useful when studying the limiting condition, which then may be expressed as,

$$F = R^2 - \boldsymbol{\varphi} \cdot \boldsymbol{\varphi}. \tag{3-32}$$

As shown in (3-29), the partial derivative is given different values depending on the sign of dF, which can be expressed as,

$$dF = -2\boldsymbol{\varphi} \cdot d\boldsymbol{\varphi}. \tag{3-33}$$

A graphical representation of the limiting condition is given in Figure 3-3. The left drawing shows the condition in $f_p - f_q$ space where $F = 0$ is indicated by the circle intersecting the axes at R and $-R$. Inside the circle $F > 0$ and outside the circle $F < 0$. The only parts "active" in the model are inside or on the circle. The current state is given by the vector $\boldsymbol{\varphi}$. At its tip two possible increments of

the vector are indicated by $d\boldsymbol{\varphi}^+$ and $d\boldsymbol{\varphi}^-$. The superposed indices indicate the sign of the scalar product $\boldsymbol{\varphi} \cdot d\boldsymbol{\varphi}$.

The right drawing in Figure 3-3 shows the limiting condition when viewing the cut A-A indicated in the left figure. The horizontal coordinate is aligned with $\boldsymbol{\varphi}$ and the vertical coordinate shows the value of F. The products $\boldsymbol{\varphi} \cdot d\boldsymbol{\varphi}^+$ and $\boldsymbol{\varphi} \cdot d\boldsymbol{\varphi}^-$, show how the difference in alignment of $d\boldsymbol{\varphi}^{\mp}$ with $\boldsymbol{\varphi}$ gives different sign of dF and, by (3-29), different values for the partial derivatives.

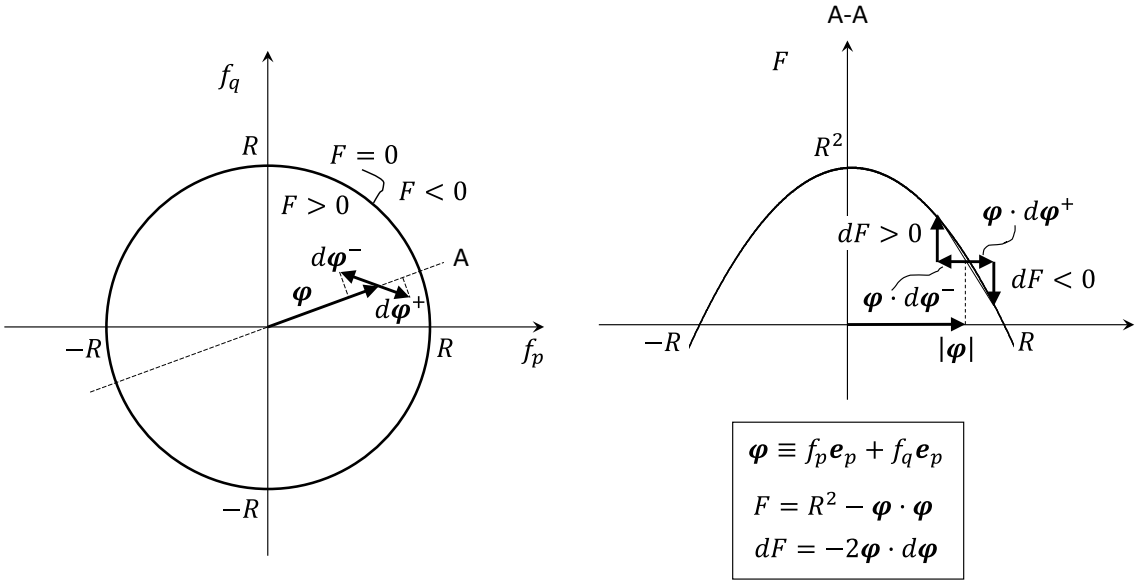

Figure 3-3. Graphical representation of the limiting condition for the path dependent variable.

It is possible to formulate the rule in (3-29) as:

- When $\boldsymbol{\varphi} \cdot d\boldsymbol{\varphi} > 0$, the stiffness tensor $\boldsymbol{K}$ is scaled with F/R^2.
- When $\boldsymbol{\varphi} \cdot d\boldsymbol{\varphi} < 0$, the stiffness tensor $\boldsymbol{K}$ is scaled with 1.

Thus, when getting closer to the limiting circle ($F = 0$) the change of the path dependent variable decreases until it becomes zero at the limit. When distancing from the limiting circle the change of the path dependent variable is maximized.

3.2.4 Micro void ratio

The evolution equation of the micro void ratio reads,

$$de_\mu = \frac{\partial e_\mu}{\partial e} de + \frac{\partial e_\mu}{\partial s} ds \,, \tag{3-34}$$

The first of the differentials describes a kinematical coupling to total void ratio and the second describe the swelling of the saturated clay grains in terms of suction. The first differential is chosen as being given by the contact area function,

$$\frac{\partial e_\mu}{\partial e} = \tilde{\alpha}(e, e_\mu), \tag{3-35}$$

and the second differential by,

$$\frac{\partial e_\mu}{\partial s} = \begin{cases} \dfrac{(e - e_\mu)\widetilde{\Psi}_M(e_\mu)}{s} \dfrac{1}{(e - e_\mu)\dfrac{\partial \widetilde{\Psi}_M}{\partial e_\mu} - \widetilde{\Psi}_M(e_\mu)} & \text{if } \dot{s} < 0 \\ \dfrac{-e_{step}}{\left| s - \widetilde{\Psi}_M(e_\mu - e_{step}) \right|} & \text{otherwise} \end{cases} . \tag{3-36}$$

The differential with respect to suction describes the swelling of the saturated clay grains. The suction differential is different for different sign of the suction rate. The expression active for drying

conditions was developed to better account for what is observed in experiments. Below follows a description of how the suction differential was formulated.

For negative suction rates, the properties of $\partial e_\mu/\partial s$ is illustrated in the left panel of Figure 3-4. The derivative is defined so that: i) the suction decreases faster than the ψ_M-function for increasing e_μ-values; and ii) so that saturated conditions (i.e., $e_\mu = e_{tot}$) is reached precisely when $s = 0$. The first condition implies that a stress which corresponds to $f = 0, (\boldsymbol{f} = f\mathbf{1})$ will display an increasing trend. This is achieved with the condition that the s/ψ_M-ratio displays a linear decrease with an increasing e_μ-value (Figure 3-4, left panel, right graph). The introduction of this ratio (r) means that:

$$s = r\Psi_M \,. \tag{3-37}$$

Taking the derivative of the expression above with respect to e_μ results in the first relation in the equation below.

$$\frac{\partial s}{\partial e_\mu} = \frac{\partial r}{\partial e_\mu}\Psi_M + r\frac{\partial \Psi_M}{\partial e_\mu} = \frac{-s}{\Psi_M}\frac{1}{e_{tot} - e_\mu}\Psi_M + \frac{s}{\Psi_M}\frac{\partial \Psi_M}{\partial e_\mu} \tag{3-38}$$

This expression is obtained by identifying $\partial r/\partial e_\mu$ as a straight line from the point (e_μ, r) to point $(e_{tot}, 0)$ in Figure 3-4 (left panel, right graph), and by substituting r with s/Ψ_M. Inverting the relation above gives the sought reciprocal partial derivative.

For positive suction rates, the properties of the corresponding derivative are illustrated in the right panel of Figure 3-4. The derivative is defined so that the suction value changes asymptotically towards the Ψ_M-function. This implies that a stress (with $f = 0$) will display an asymptotic trend towards zero.

For this purpose, a parameter e_{step} is introduced. The derivative is defined so that a stress path in each point (e_μ, s) is directed towards the point $\left(e_\mu - e_{step}, \widetilde{\Psi}_M(e_\mu - e_{step})\right)$ which yields the following expression:

$$\frac{\partial e_\mu}{\partial s} = \frac{-e_{step}}{\left|s - \widetilde{\Psi}_M(e_\mu - e_{step})\right|}. \tag{3-39}$$

Since e_{step} is constant, this means that the point of direction will change with decreasing e_μ values. The absolute value is introduced so that the derivative will yield a negative value regardless of the relative magnitude of s and Ψ_M.

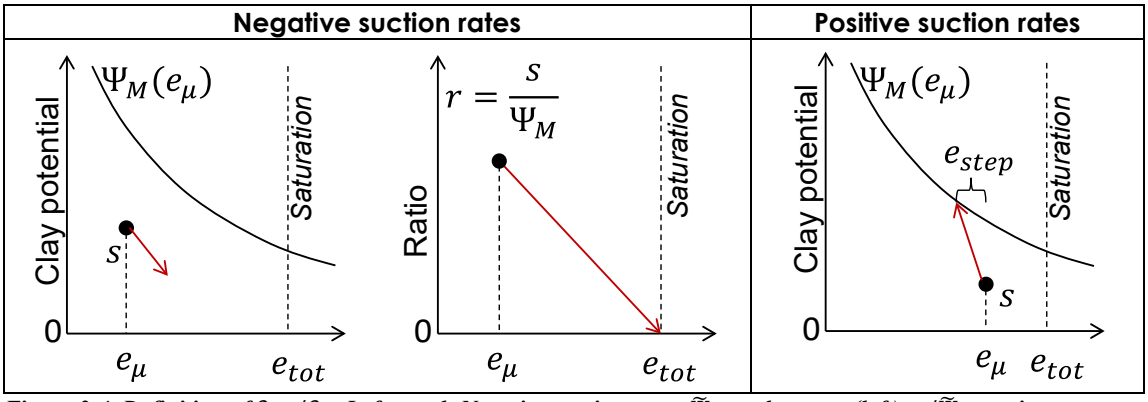

Figure 3-4. Definition of $\partial e_\mu/\partial s$. Left panel: Negative suction rates, $\widetilde{\Psi}_M$ and s vs e_μ (left); $s/\widetilde{\Psi}_M$- ratio vs. e_μ (right). Right panel: Positive suction rates, $\widetilde{\Psi}_M$ and s vs. e_μ.

4 Implementation in COMSOL®

When implementing the HBM formulation in COMSOL Multipysics® the mass balances were implemented using a general partial differential equation (PDE) interface, the stress balance was incorporated by using the available solid mechanics interface and mechanical constitutive relations were specified using a distributed ordinary differential equation (DODE) interface.

The mass balance equations have been implemented in two different ways, both considered to be proper, see section 4.1. Either with the *mass balances implemented separately*, or in a *combined equation system*. Whether one of the implementations is to be preferred before the other has not yet been established. The combined implementation was developed trying to improve convergency.

Simple constitutive functions, such as $\tilde{\rho}_l(s) = {\rho_l}^0 \exp(-\alpha s)$, were, on recommendation from COMSOL® developers, implemented as variables rather than functions. Variable representation is apparently closer to what the algorithm uses internally.

Constitutive relations on rate form, present in the mechanical part of the model, e.g., $\dot{\boldsymbol{\sigma}} = \mathbb{C}\,\dot{\boldsymbol{\varepsilon}} + \mathbb{d}\,\dot{s}$, implemented as DODEs, is discussed in section 4.2.

When using the PDE and DODE interfaces, the discretization must be defined by specifying three quantities, shape function type, element order, and frame.

- Shape function type: Lagrangean except for $\boldsymbol{\sigma}$ and $\boldsymbol{f}$ where discontinuous Lagrangean were used. It has not yet been understood why discontinuous function should work better, but so has been the case.
- Element order: Displacements uses cubic, and the rest is using quadratic.
- Frame: Material frame was used for all cases.

4.1 Solid and liquid water mass balance

When describing the implementation of the water mass balance, only the liquid water mass balance is considered for clarity and readability. In COMSOL® there is an option of implementing a general form PDE which reads,

$$e_a \frac{\partial^2 u}{\partial t^2} + d_a \frac{\partial u}{\partial t} + \nabla \cdot \Gamma = f\,. \tag{4-1}$$

For HBM $e_a = 0$ has been used, which results in,

$$d_a \frac{\partial u}{\partial t} + \nabla \cdot \Gamma = f\,. \tag{4-2}$$

This equation may be multidimensional, the ingoing entities might be arrays of different orders and dimensions. When formulating an axisymmetric problem, the divergence operator is not correctly represented in COMSOL®. This was, in the case of the water mass balance, compensated for by adding the term,

$$-\frac{\rho_l \boldsymbol{q}_l}{R}, \tag{4-3}$$

to the right-hand side. This is explained in the COMSOL® reference manual (2022) under equation-based modelling.

The formulation has the water and solid mass balances given in subsections 2.2 and 3.1, which are repeated below,

$$(1-\phi)\dot{\overline{\rho_l e_\mu}} + \operatorname{div}(\rho_l \boldsymbol{q}_l) = {f_l}^w \tag{4-4}$$

$$(1-\phi)\dot{e} = \dot{\varepsilon}_v \tag{4-5}$$

The time derivative in the water mass balance can be expressed in terms of time derivatives of void ratio and suction using that,

$$\dot{\rho}_l = \frac{\partial \rho_l}{\partial \mathrm{s}} \dot{s} \tag{4-6}$$

$$\dot{e}_\mu = \frac{\partial e_\mu}{\partial e} \dot{e} + \frac{\partial e_\mu}{\partial \mathrm{s}} \dot{\mathrm{s}} \tag{4-7}$$

so that the balance equations take the form,

$$(1-\phi)\left(e_\mu \frac{\partial \rho_l}{\partial \mathrm{s}} + \rho_l \frac{\partial e_\mu}{\partial \mathrm{s}} \right) \dot{s} + \ \mathrm{div}(\rho_l \boldsymbol{q}_l) = {f_l}^w - (1-\phi)\rho_l \frac{\partial e_\mu}{\partial e} \dot{e} \tag{4-8}$$

$$(1-\phi)\dot{e} = \dot{\varepsilon}_v \tag{4-9}$$

The two balance equations can be *solved separately* if choosing,

$$u^l = s \, , u^s = e \, , \tag{4-10}$$

and identify,

$${d_a}^l = (1-\phi)\left(e_\mu \frac{\partial \rho_l}{\partial \mathrm{s}} + \rho_l \frac{\partial e_\mu}{\partial \mathrm{s}} \right) , {d_a}^s = (1-\phi) \tag{4-11}$$

$$\boldsymbol{\Gamma}^l = \rho_l \boldsymbol{q}_l \, , \boldsymbol{\Gamma}^s = \mathbf{0} \tag{4-12}$$

$$f^l = {f_l}^w - (1-\phi)\rho_l \frac{\partial e_\mu}{\partial e} \dot{e} \, , f^s = \dot{\varepsilon}_v \, . \tag{4-13}$$

The two balance equations can also be *solved together* in a combined equation system if choosing,

$$\boldsymbol{u} = [s \quad e]^T \, . \tag{4-14}$$

The following can then be identified,

$$\boldsymbol{d}_a = \begin{bmatrix} (1-\phi)\left(e_\mu \frac{\partial \rho_l}{\partial \mathrm{s}} + \rho_l \frac{\partial e_\mu}{\partial \mathrm{s}} \right) & (1-\phi)\left(\rho_l \frac{\partial e_\mu}{\partial e} \right) \\ 0 & (1-\phi) \end{bmatrix}, \tag{4-15}$$

$$\boldsymbol{\Gamma} = \begin{bmatrix} \rho_l \boldsymbol{q}_l \\ \mathbf{0} \end{bmatrix}, \tag{4-16}$$

$$\boldsymbol{f} = \begin{bmatrix} {f_l}^w \\ \dot{\varepsilon}_v \end{bmatrix}. \tag{4-17}$$

4.2 Mechanics

The total stress of HBM must be inserted in the quasistatic balance of momentum (balance of stress),

$$\mathrm{div}\boldsymbol{\sigma} + \boldsymbol{b} = \mathbf{0} \, , \tag{4-18}$$

which in COMSOL® is available through using the solid mechanics interface. The total stress of HBM is introduced in (4-18) by using an external stress contribution to a linear elastic material. The elastic material itself is "deactivated" by adopting zero stiffness.

To implement the mechanical constitutive equations in COMSOL® the DODE interface is used. The constitutive relations are defined by evolution equations of; total stress, the internal path dependent variable, and the micro void ratio, given by,

$$\dot{\boldsymbol{\sigma}} = \mathbb{C} \, \dot{\boldsymbol{\varepsilon}} + \mathbb{d} \, \dot{s} \, , \qquad \dot{\boldsymbol{f}} = \frac{\partial \boldsymbol{f}}{\partial \boldsymbol{\varepsilon}} \dot{\boldsymbol{\varepsilon}} \, , \qquad \text{and } \dot{e}_\mu = \frac{\partial e_\mu}{\partial e} \dot{e} + \frac{\partial e_\mu}{\partial \mathrm{s}} \dot{\mathrm{s}} \, , \tag{4-19}$$

respectively.

As chapter 2.3 shows, the relation describing the total stress is not formulated on rate form. The derivation to get this is given in Appendix F and the result is given below using index notation. The total stress rate is given by,

$$\dot{\sigma}_{ij} = C_{ijkl} \dot{\varepsilon}_{kl} + d_{ij} \dot{s} \, , \tag{4-20}$$

where,

$$C_{ijkl} = \alpha {C^I}_{ijkl} + a^{\varepsilon} {\sigma^I}_{ij} \delta_{kl} \,, \tag{4-21}$$

$${C^I}_{ijkl} = -(1+e)\frac{\partial e_\mu}{\partial e}\left(\frac{\partial \Psi_M}{\partial e_\mu}\delta_{ij} + \frac{\partial \Psi_\Delta}{\partial e_\mu} f_{ij}\right)\delta_{kl} - \Psi_\Delta \frac{\partial f_{ij}}{\partial \varepsilon_{kl}}, \tag{4-22}$$

$$a^{\varepsilon} = \left(\frac{\partial \alpha}{\partial e} + \frac{\partial \alpha}{\partial e_\mu}\frac{\partial e_\mu}{\partial e}\right)(1+e)\,, \tag{4-23}$$

and

$$d_{ij} = \alpha {d^I}_{ij} + a^s {\sigma^I}_{ij}\,, \tag{4-24}$$

$${d^I}_{ij} = \delta_{ij} - \frac{\partial e_\mu}{\partial s}\left(\frac{\partial \Psi_M}{\partial e_\mu}\delta_{ij} + \frac{\partial \Psi_\Delta}{\partial e_\mu} f_{ij}\right), \tag{4-25}$$

$$a^s = \frac{\partial \alpha}{\partial e_\mu}\frac{\partial e_\mu}{\partial s}\,. \tag{4-26}$$

As described in chapter 3.2.3, the partial differential, $\partial \boldsymbol{f}/\partial \boldsymbol{\varepsilon}$, in the evolution equation of the path dependent variable, is dependent on the sign of the rate of the limiting condition function F. A strain driven format of the evolution equation of the path dependent variable has been derived, see Appendix G. The resulting algorithm reads,

$$\text{if } \left[\left(\frac{7}{3} f_p\, \mathbf{1} - 3\boldsymbol{f}\right)\cdot(-\boldsymbol{K}\dot{\boldsymbol{\varepsilon}}) \geq 0\right] \text{ then } \frac{\partial \boldsymbol{f}}{\partial \boldsymbol{\varepsilon}} = -\boldsymbol{K}\,, \qquad \text{else } \frac{\partial \boldsymbol{f}}{\partial \boldsymbol{\varepsilon}} = -\frac{F}{R^2}\boldsymbol{K}\,. \tag{4-27}$$

It could also be mentioned that to get a numerically convenient formulation of the micro void ratio evolution equation, the partial derivative with respect to suction has been multiplied with a smooth step function so that it goes to zero when suction < 0.

In COMSOL®, the distributed ordinary differential equations are given on the format,

$$\boldsymbol{e}_a \frac{\partial^2 \boldsymbol{u}}{\partial t^2} + \boldsymbol{d}_a \frac{\partial \boldsymbol{u}}{\partial t} = \boldsymbol{r}\,. \tag{4-28}$$

Using $\boldsymbol{e}_a = \boldsymbol{0}$ and $\boldsymbol{d}_a = [\delta_{ij}]$ gives,

$$\frac{\partial \boldsymbol{u}}{\partial t} = \boldsymbol{r}\,. \tag{4-29}$$

The identification of $\boldsymbol{u}$ and $\boldsymbol{r}$ in the three systems of ordinary differential equations is given in Table 4-1.

Table 4-1 Identification of u and r in the mechanical constitutive equations.

	$\dot{\boldsymbol{\sigma}} = \mathbb{C}\,\dot{\boldsymbol{\varepsilon}} + \mathbb{d}\,\dot{s}$	$\dot{\boldsymbol{f}} = \frac{\partial \boldsymbol{f}}{\partial \boldsymbol{\varepsilon}}\dot{\boldsymbol{\varepsilon}}\,,$	$\dot{e}_\mu = \frac{\partial e_\mu}{\partial e}\dot{e} + \frac{\partial e_\mu}{\partial \mathrm{s}}\dot{\mathrm{s}}$
$\boldsymbol{u}$	$[\sigma_{11}, \sigma_{22}, \sigma_{33}, \sigma_{12}, \sigma_{13}, \sigma_{23}]^{\mathrm{T}}$	$[f_{11}, f_{22}, f_{33}, f_{12}, f_{13}, f_{23}]^{\mathrm{T}}$	e_μ
$\boldsymbol{r}$	$\mathbb{C}\,\dot{\boldsymbol{\varepsilon}} + \mathbb{d}\,\dot{s}$	$\frac{\partial \boldsymbol{f}}{\partial \boldsymbol{\varepsilon}}\dot{\boldsymbol{\varepsilon}}$	$\frac{\partial e_\mu}{\partial e}\dot{e} + \frac{\partial e_\mu}{\partial \mathrm{s}}\dot{\mathrm{s}}$

5 Final comments

One of the main insights gained from evaluating the work in the BEACON project was that the HBM model agrees well with how bentonite behaves in a variety of different cases using a single set of parameters identified from experimental data. There seems to be significantly less need for tweaking the parameter set when modelling different cases using HBM as compared to when using the material models Clay Technology usually utilize.

These properties indicates that HBM is based on a proper description of bentonite's behaviour and that it is well worth to continue working with this formulation. Thermodynamics and mixture theory are also common parts when describing bentonite's behaviour and using these as a basis provide possibilities to generalize the model so that it also can incorporate dependencies on groundwater salinity, ion-exchange, ion-transport, freezing, etc.

The main and most important part of the parameter set is used for representing the clay potential which is directly linked to characteristic material properties of bentonite such as swelling pressure curves and retention curves. To obtain an accurate representation of the material it is crucial to parametrize and calibrate the clay potential functions so that they agree with the characteristic material properties. The need for reliable experimental data is also obvious.

The HBM formulation is at the time of writing this report still in a phase of development. The basis of the formulation is, however, considered to be suitable for the application, and it is flexible enough to provide different possibilities on how to describe the material behaviour. An example of this is the novel description of the evolution equation for the path-dependent variable. The new variant is less complex and seems to be numerically favourable. A recent accomplishment: progress in solving problems including HBM and wall friction, which is known to be numerically demanding, indicates that this is the case.

The ability to use friction and contact mechanics is important and it has therefore been a long-term goal of the project to be able to address problems where friction and HBM is solved together. Several unsuccessful attempts have been made during the project, but it was not until a new version of the expression for the path-dependent variable had been implemented that first steps towards this were made. Even with this new expression, which seem to increase the numerical stability of HBM, the simulation was not possible to run in its entirety.

A stepwise strategy was used to find an initially convergent model setup with HBM and wall friction. First, a simulation where wall friction was solved together with a very simple mechanical material model was constructed and solved. The mechanical material model was then exchanged for BBM, available within the COMSOL® software, and a new suitable setting of the friction properties and numerical solver was sought to obtain convergence. This procedure was continued in small steps until an initially convergent simulation with HBM and wall friction had been found. In this way some knowledge of the settings, suitable for solving problems including friction, was gained throughout the process and a good starting point for including HBM was achieved.

There is often an initial phase of "resistance" when starting to use a new software. This was not different in the case of COMSOL Multiphysics®, where a lot of new components had to be understood: a new graphical interface, the structure and inner workings of the code, capabilities/interfaces of different physics modules, selecting solvers, setting up numerical tolerances, etc. There often was a need for rewriting the formulation on a format which allowed for, and/or simplified, the implementation. In the case of HBM, the entire mechanical material model is formulated on a rate form driven by strain and suction. Both the stress relation and the relation for the path-dependent variable have been rewritten on rate forms.

At present the implementation of HBM in COMSOL® is carried out in a straightforward way using modules accessible through the graphical interface. It should however be understood that the only utilized part within COMSOL® representing an actual physics module is the solid mechanics interface where the stress equilibrium is represented, and within this the material model is deactivated. For the rest of the implementation purely mathematical interfaces for partial differential equations and distributed ordinary differential equations are used.

Below some suggestions for future work are listed:

- HBM contains non-linear functions and discrete formulations which makes it a difficult task for the solver. The usability of the model, for example improving concurrent use of friction mechanics, could be enhanced if it was possible to "linearize" and making the formulation "smoother". The recent development regarding the path dependent variable is an example of such smoothing.
- Investigate different ways to couple micro to macro. Could there be another way to describe the micro to macro coupling than the presently used micro void ratio evolution equation? There might be insights to be gained from studying the homogenized framework.
- Incorporate a check that the state obtained by integration of the rate formulation meet the direct formulation $-\boldsymbol{\sigma}^{\mathrm{I}} = \boldsymbol{\Psi} - s\mathbf{1}$.
- HBM-module within COMSOL®. At the time being the implementation of HBM occupies a large part of and is spread throughout the COMSOL® interface. It could therefore be beneficial to develop an "HBM-module" within COMSOL® to simplify use and give a better overview of models incorporating HBM.

References

SKB's (Svensk Kärnbränslehantering AB) publications can be found at www.skb.com/publications. SKBdoc documents will be submitted upon request to document@skb.se.

Börgesson L, Åkesson M, Hernelind J, 2020. EBS TF – THM modelling, Homogenisation task. SKB P-18-05, Svensk Kärnbränslehantering AB.

COMSOL Reference Manual, 2022. COMSOL Multiphysics® v. 6.1. Stockholm: COMSOL AB, 1208-1209.

Dueck A, Börgesson L, Kristensson O, Malmberg D, Åkesson M, Hernelind J, 2019. Bentonite homogenisation - Laboratory study, model development and modelling of homogenisation processes. SKB TR-19-11, Svensk Kärnbränslehantering AB.

Larsson R, 2012. Continuum mechanics of two-phase porous media. Division of material and computational mechanics. In Computational continuum mechanics of porous materials. Göteborg, 15 December 2012. Göteborg: Chalmers University of Technology.

Gens A, 2018. BEACON deliverable D3.1 Description of the constitutive models available at the start of the project. Conceptual bases, mathematical description and capabilities and shortcomings. European commission.

Gens A, 2020. BEACON deliverable D3.2 Description of the improved constitutive models and their implementation and verification. European commission.

Gens A, 2021. BEACON deliverable D3.3 Description of the constitutive models developed in the project. Conceptual bases, mathematical description and model capabilities. Assessment of predictive power. European commission.

Talandier J, 2019. BEACON deliverable D5.1.2 Synthesis of results from task 5.1. European commission.

Talandier J, 2020a. BEACON deliverable D5.2.2 Synthesis of results from task 5.2. European commission.

Talandier J, 2020b. BEACON deliverable D5.3.2 Synthesis of results from task 5.3. European commission.

Charlier R, Darde B, Talandier J, 2021. BEACON deliverable D5.6 Specifications for Beacon WP5: Testing, verification and validation of models, Step 3 – predictive test cases. European commission.

Talandier J, Kristensson O, Malmberg D, Narkuniene A, Justinavicius D, Zdravkovic L, Pulkkanen V-M, Gharbieh H, Ferrari A, Bosch Llufriu J, Kumar V, Beese S, Gens A, Charlier R, Newson R, Åkesson M, Scaringi G, Masin D, Leupin O, 2022. BEACON deliverable D5.7 Synthesis of the results obtained from all tasks in WP5, Final report for WP5. European commission.

Appendix A: Theoretical framework

To set the stage properly for the description of the material model, the theoretical framework in which this is formulated is described below.

Index free notation is used to the major part, but sometimes index notation is used. A Cartesian coordinate frame, consisting of a reference point (the origin) and a positive orthonormal basis $\{\boldsymbol{e}_1, \boldsymbol{e}_2, \boldsymbol{e}_3\}$, is used. Using this a vector $\boldsymbol{v}$ can be expressed,

$$\boldsymbol{v} = v_1\boldsymbol{e}_1 + v_2\boldsymbol{e}_2 + v_2\boldsymbol{e}_2 = v_i\boldsymbol{e}_i \tag{A-1}$$

and a second order tensor $\boldsymbol{T}$ can be expressed as,

$$\boldsymbol{T} = \begin{matrix} T_{11}\boldsymbol{e}_1 \otimes \boldsymbol{e}_1 + T_{12}\boldsymbol{e}_1 \otimes \boldsymbol{e}_2 + T_{13}\boldsymbol{e}_1 \otimes \boldsymbol{e}_3 + \\ T_{21}\boldsymbol{e}_2 \otimes \boldsymbol{e}_1 + T_{22}\boldsymbol{e}_2 \otimes \boldsymbol{e}_2 + T_{23}\boldsymbol{e}_2 \otimes \boldsymbol{e}_3 + = T_{ij}\boldsymbol{e}_i \otimes \boldsymbol{e}_j\,, \\ T_{31}\boldsymbol{e}_3 \otimes \boldsymbol{e}_1 + T_{32}\boldsymbol{e}_3 \otimes \boldsymbol{e}_2 + T_{33}\boldsymbol{e}_3 \otimes \boldsymbol{e}_3 \end{matrix} \tag{A-2}$$

where $\otimes$ denote the tensor product between vectors so that $\boldsymbol{e}_i \otimes \boldsymbol{e}_j$ is a second order tensor. As can be seen in the right-hand sides above, summation convention is used to compress the index notation. The second order unit tensor $\mathbf{1}$ is defined by $\mathbf{1}\boldsymbol{v} = \boldsymbol{v}$, and the following is used when using index notation,

$$\mathbf{1} = \delta_{ij}\boldsymbol{e}_i \otimes \boldsymbol{e}_j\,, \delta_{ij} = \begin{cases} 1 \text{ if } i = j \\ 0 \text{ if } i \neq j \end{cases}. \tag{A-3}$$

For a single-phase continuum, position vectors $\boldsymbol{X}$ of material particles in a body in its reference configuration $\mathcal{B}_0$ together with a function $\boldsymbol{\chi}$, describing the motion of the points, give position vectors $\boldsymbol{x} = \boldsymbol{\chi}(\boldsymbol{X}, t)$, in the current configuration $\mathcal{B}$. For a fixed time, the inverse mapping $\boldsymbol{X} = \boldsymbol{\chi}^{-1}(\boldsymbol{x}, t)$ exists. Displacements are defined by $\boldsymbol{u} = \boldsymbol{x} - \boldsymbol{X}$.

Taking the partial time derivative of the motion gives the velocity,

$$\boldsymbol{v}(\boldsymbol{X}, t) = \frac{\partial \boldsymbol{\chi}(\boldsymbol{X}, t)}{\partial t} \tag{A-4}$$

which, by using the inverse map, also can be given by,

$$\boldsymbol{v}(\boldsymbol{x}, t) = \frac{\partial \boldsymbol{\chi}(\boldsymbol{\chi}^{-1}(\boldsymbol{x}, t), t)}{\partial t}. \tag{A-5}$$

In line with the above, fields may be defined over the body in both configurations, thus a field φ may be given as $\varphi(\boldsymbol{X}, t)$ or $\varphi(\boldsymbol{x}, t)$, being the material description and spatial description, respectively.

The material time derivative $\dot{\varphi}$ and spatial time derivative $\acute{\varphi}$ of the φ-field are defined by:

$$\dot{\varphi}(\boldsymbol{X}, t) = \frac{\partial \varphi(\boldsymbol{X}, t)}{\partial t} \text{ (holding } \boldsymbol{X} \text{ fixed)}\,, \tag{A-6}$$

and

$$\acute{\varphi}(\boldsymbol{x}, t) = \frac{\partial \varphi(\boldsymbol{x}, t)}{\partial t} \text{ (holding } \boldsymbol{x} \text{ fixed)}\,, \tag{A-7}$$

respectively. When φ is a spatial field (given in terms of $\boldsymbol{x}$) its material time derivative is given by,

$$\dot{\varphi}(\boldsymbol{x}, t) = \acute{\varphi}(\boldsymbol{x}, t) + \frac{\partial \varphi(\boldsymbol{x}, t)}{\partial \boldsymbol{x}} \cdot \boldsymbol{v}(\boldsymbol{x}, t)\,. \tag{A-8}$$

The deformation gradient,

$$\boldsymbol{F} = \frac{\partial \boldsymbol{x}}{\partial \boldsymbol{X}} = \frac{\partial (\boldsymbol{X} + \boldsymbol{u})}{\partial \boldsymbol{X}} = \mathbf{1} + \frac{\partial \boldsymbol{u}}{\partial \boldsymbol{X}}, \tag{A-9}$$

is a kinematical entity linking an infinitesimal material fibre $d\boldsymbol{X}$ in the reference (undeformed) configuration to an infinitesimal material fiber $d\boldsymbol{x}$ in the deformed configuration. The determinant of $\boldsymbol{F}$ links a volume element in the reference configuration dV to a volume element in the current configuration dv,

$$dv = \det\boldsymbol{F}\, dV = \mathrm{J}\, dV\,. \tag{A-10}$$

We also have the useful relation,

$$\frac{\dot{\mathrm{J}}}{\mathrm{J}} = \mathrm{div}\boldsymbol{v}\,. \tag{A-11}$$

The model in this work uses a mixture formulation consisting of several phases α which are superimposed upon each other. This leads to several position vectors $\boldsymbol{X}^\alpha$ of material points belonging to different reference configurations ${\mathcal{B}_0}^\alpha$ together with functions $\boldsymbol{\chi}^\alpha$ describing the motion of the points which results in a position vector $\boldsymbol{x} = \boldsymbol{\chi}^\alpha(\boldsymbol{X}^\alpha, t)$ belonging to the current configuration. This leads to velocities,

$$\boldsymbol{v}^\alpha = \frac{D^\alpha \boldsymbol{x}}{Dt} = \frac{\partial \boldsymbol{\chi}^\alpha(\boldsymbol{X}^\alpha, t)}{\partial t}, \tag{A-12}$$

where $D^\alpha()/Dt$ is a compact notation of a material derivative with respect to reference configuration ${\mathcal{B}_0}^\alpha$.

Now consider the case where there are two immiscible phases: a solid phase (*s*) and a fluid phase (*f*). The immiscibility makes it possible to define phase volumes $V^s + V^f = V$ and volume fractions $n^s = V^s/V$ and $n^f = V^f/V$.

The solid phase is chosen as the referential phase and therefore we identify $\mathcal{B}_0 = {\mathcal{B}_0}^s$, $\boldsymbol{X} = \boldsymbol{X}^s$, $\boldsymbol{\chi}(\boldsymbol{X}, t) = \boldsymbol{\chi}^s(\boldsymbol{X}^s, t)$, $\boldsymbol{v} = \boldsymbol{v}^\mathrm{s}$, thus,

$$\boldsymbol{v} = \boldsymbol{v}^\mathrm{s} = \frac{D^s \boldsymbol{x}}{Dt} = \dot{\boldsymbol{\chi}}(\boldsymbol{X}, t)\,, \tag{A-13}$$

where the "dot derivative" is introduced and defined as the material derivative with respect to the solid reference configuration.

All the kinematics described for a single-phase formulation are therefore now describing the solid phase kinematics. A relative velocity $\boldsymbol{v}^r = \boldsymbol{v}^f - \boldsymbol{v}^s$ and a Darcian velocity $\boldsymbol{v}^d = n^f \boldsymbol{v}^r$ can be introduced.

In this paragraph a definition of the small strain tensor $\boldsymbol{\varepsilon}$ and the underlying approximation made is given. The Lagrangean (large) strain tensor,

$$\boldsymbol{E} = \frac{1}{2}(\boldsymbol{F}^T\boldsymbol{F} - \boldsymbol{1})\,, \tag{A-14}$$

is used as a basis for describing the small strain approximation. Using the relation between the deformation gradient and the displacement gradient makes it possible to write,

$$\boldsymbol{E} = \frac{1}{2}\left(\left(\boldsymbol{1} + \frac{\partial \boldsymbol{u}}{\partial \boldsymbol{X}}\right)^T\left(\boldsymbol{1} + \frac{\partial \boldsymbol{u}}{\partial \boldsymbol{X}}\right) - \boldsymbol{1}\right) = \frac{1}{2}\left(\frac{\partial \boldsymbol{u}}{\partial \boldsymbol{X}} + \left(\frac{\partial \boldsymbol{u}}{\partial \boldsymbol{X}}\right)^T + \left(\frac{\partial \boldsymbol{u}}{\partial \boldsymbol{X}}\right)^T\frac{\partial \boldsymbol{u}}{\partial \boldsymbol{X}}\right). \tag{A-15}$$

If the displacement gradient is small, i.e. $\partial \boldsymbol{u}/\partial \boldsymbol{X} = \boldsymbol{F} - \boldsymbol{1}$ is small, the last higher order term of the Lagrangean strain tensor becomes insignificant in relation to the first order terms. The Lagrangean strain may then be approximated by the small (infinitesimal) strain:

$$\boldsymbol{E} \approx \boldsymbol{\varepsilon} \equiv \frac{1}{2}\left(\frac{\partial \boldsymbol{u}}{\partial \boldsymbol{X}} + \left(\frac{\partial \boldsymbol{u}}{\partial \boldsymbol{X}}\right)^T\right) = \frac{1}{2}(\boldsymbol{F} + \boldsymbol{F}^T) - \boldsymbol{1}. \tag{A-16}$$

As can be seen, conventional continuum mechanics sign conventions are adopted, when a material fiber undergoes elongation strain is positive. The same pass for stresses $\boldsymbol{\sigma}$ being positive for tensile conditions.

The stress and strain tensors can be decomposed in a spherical part and a deviatoric part according to,

$$\boldsymbol{\sigma} = \frac{1}{3}\mathrm{tr}\boldsymbol{\sigma}\,\boldsymbol{1} + \boldsymbol{s} = -p\,\boldsymbol{1} + \boldsymbol{s} \quad \text{and} \quad \boldsymbol{\varepsilon} = \frac{1}{3}\mathrm{tr}\boldsymbol{\varepsilon}\,\boldsymbol{1} + \boldsymbol{e} = \frac{1}{3}\varepsilon_v\,\boldsymbol{1} + \boldsymbol{e}\,, \tag{A-17}$$

where tr denotes the trace of the tensor, i.e. $\mathrm{tr}\boldsymbol{\sigma} = \boldsymbol{\sigma} \cdot \boldsymbol{1}$.

Pressure, p, (positive in compression) and volumetric strain, ε_v, (positive for an increase in volume) are defined using the spherical part of the tensors according to,

$$p \equiv -\frac{1}{3}\mathrm{tr}\boldsymbol{\sigma} \quad \text{and} \quad \varepsilon_v \equiv \mathrm{tr}\boldsymbol{\varepsilon}\,, \tag{A-18}$$

respectively.

In the following a tilde above an entity indicate that the entity should be considered a function, i.e.

$$\alpha = \tilde{\alpha}(a, b) \tag{A-19}$$

should be understood as the variable α is given by the function $\tilde{\alpha}$ having the input variables a and b.

Reynold's transport relation will be used in the derivations, when applied to a field $\psi(\boldsymbol{x}, t)$, it reads,

$$\frac{d}{dt}\left(\int_{\mathcal{B}} \psi(\boldsymbol{x}, t) dv(\boldsymbol{x})\right) = \int_{\mathcal{B}} \left(\dot{\psi} + \psi \mathrm{div}\boldsymbol{v}\right) dv\,, \tag{A-20}$$

and the relation,

$$\begin{aligned} \mathrm{div}\boldsymbol{v} = \mathrm{tr}\left(\frac{\partial \dot{\boldsymbol{\chi}}(\boldsymbol{\chi}^{-1}(\boldsymbol{x}, t), t)}{\partial \boldsymbol{x}}\right) = \frac{\partial}{\partial t}\mathrm{tr}\left(\frac{\partial \boldsymbol{\chi}(\boldsymbol{X}, t)}{\partial \boldsymbol{x}}\right) = \frac{\partial}{\partial t}\mathrm{tr}\left(\frac{\partial(\boldsymbol{u} + \boldsymbol{X})}{\partial \boldsymbol{x}}\right) \\ = \frac{\partial}{\partial t}\mathrm{tr}\left(\frac{\partial \boldsymbol{u}}{\partial \boldsymbol{x}}\right) = \frac{\partial}{\partial t}(\mathrm{tr}\boldsymbol{\varepsilon}) = \dot{\varepsilon}_v\,, \end{aligned} \tag{A-21}$$

is therefore often also valuable.

Appendix B: Solid mass balance

The solid mass per mixture volume can be expressed,

$$\frac{dm_s}{dv} = \frac{dm_s}{dv_s}\frac{dv_s}{dv} = \rho_s(1-\phi). \tag{B-1}$$

The total solid mass $\mathcal{M}^s$ is obtained from integrating the expression above over the body in its current configuration $\mathcal{B}$. The integral can also be pulled back to the reference configuration of the body $\mathcal{B}_0$, thus,

$$\mathcal{M}^s = \int_{\mathcal{B}} \rho_s(1-\phi)dv = \int_{\mathcal{B}_0} \rho_s(1-\phi)JdV = \int_{\mathcal{B}_0} M_s dV \ . \tag{B-2}$$

To do this it has been used that $dv = J\,dV$, see Appendix A. Taking the time derivative with respect to the solids reference configuration gives,

$$\frac{D^s\mathcal{M}^s}{Dt} = \dot{\mathcal{M}}^s = \int_{\mathcal{B}_0} \dot{M}_s dV = 0\,. \tag{B-3}$$

Thus, the local form of the solid mass balance is given by,

$$\dot{M}_s = \overline{\rho_s(1-\phi)J} = \dot{\rho}_s(1-\phi)J - \rho_s\dot{\phi}J + \rho_s(1-\phi)\dot{J} = 0\,, \tag{B-4}$$

and assuming that ρ_s is constant gives,

$$\dot{\mathcal{M}}^s = \rho_s\int_{\mathcal{B}_0}\frac{\dot{M}_s}{\rho_s}dV = \rho_s\int_{\mathcal{B}_0}\left(-\dot{\phi}J + (1-\phi)\dot{J}\right)dV = 0\,, \tag{B-5}$$

$$\rho_s\int_{\mathcal{B}_0}\left(-\dot{\phi} + (1-\phi)\frac{\dot{J}}{J}\right)JdV = \rho_s\int_{\mathcal{B}_0}\left(-\dot{\phi} + (1-\phi)\mathrm{div}\boldsymbol{v}\right)JdV = 0\,. \tag{B-6}$$

The local condition reads,

$$\left(-\dot{\phi} + (1-\phi)\mathrm{div}\boldsymbol{v}\right)J = 0 \tag{B-7}$$

which, since $J > 0$, can be simplified to,

$$-\dot{\phi} + (1-\phi)\mathrm{div}\boldsymbol{v} = 0\,. \tag{B-8}$$

If reformulating this, we obtain,

$$\dot{\phi} = (1-\phi)\frac{\dot{J}}{J} = (1-\phi)\mathrm{div}\boldsymbol{v} \ \Rightarrow \dot{e} = (1+e)\frac{\dot{J}}{J} = (1+e)\mathrm{div}\boldsymbol{v}\,. \tag{B-9}$$

Since $\dot{M}_s = 0$, it also follows that $M_s = M_{s_0}$ which gives,

$$(1-\phi)J = 1-\phi_0 \ \Rightarrow \ 1+e = (1+e_0)J\,. \tag{B-10}$$

We can formulate the following three relations for updating the void ratio using the volumetric strain, but only the first one is proper,

$$\mathrm{div}\boldsymbol{v} = \dot{\varepsilon}_v \Rightarrow \ \dot{e} = (1+e)\dot{\varepsilon}_v\,, \tag{B-11}$$

$$J - 1 = \frac{dv - dV}{dV} \approx \varepsilon_v \Rightarrow 1 + e \approx (1+e_0)(\varepsilon_v + 1), \tag{B-12}$$

$$\dot{J} \approx \dot{\varepsilon}_v \Rightarrow \dot{e} \approx (1+e_0)\dot{\varepsilon}_v\,, \tag{B-13}$$

Appendix C: Balance of water mass

The water mass per mixture volume is given by an addition of the contributions from the liquid and gaseous phase, i.e.,

$$\frac{dm^w}{dv} = \frac{dm_l{}^w}{dv} + \frac{dm_g{}^w}{dv}. \tag{C-1}$$

For readability, the derivation of the balance of water is given separately for the two phases.

Liquid water
The liquid water mass per mixture volume can be expressed as,

$$\frac{dm_l{}^w}{dv} = \frac{dm_l{}^w}{dv_l{}^w}\frac{dv_l{}^w}{dv_s}\frac{dv_s}{dv} = \rho_l e_\mu (1-\phi) \tag{C-2}$$

The total liquid water mass $\mathcal{M}^l$ is obtained from,

$$\mathcal{M}^l = \int_{\mathcal{B}} \rho_l e_\mu (1-\phi) dv = \int_{\mathcal{B}_0} \rho_l e_\mu (1-\phi) J dV = \int_{\mathcal{B}_0} M_l dV \ , \tag{C-3}$$

where a pull-back operation has been made, i.e., the integral is first performed in the current configuration, $\mathcal{B}$, but is "pulled back" to the reference configuration, $\mathcal{B}_0$. To do this it has been used that $dv = J\, dV$, see Appendix A.

Taking the time derivative with respect to the liquid reference configuration, and performing a series of pull-back to the liquid reference ${\mathcal{B}^l}_0$, push-forward to the current configuration, $\mathcal{B}$, and finally a pull-back to the solid reference configuration, $\mathcal{B}_0$, we have,

$$\begin{aligned}
\frac{D^l \mathcal{M}^l}{Dt} = \frac{D^l}{Dt}\int_{\mathcal{B}} \rho_l e_\mu (1-\phi) dv &= \frac{D^l}{Dt}\int_{{\mathcal{B}^l}_0} \rho_l e_\mu (1-\phi) J^l dV \\
&= \int_{{\mathcal{B}^l}_0} \frac{D^l}{Dt}\left(\rho_l e_\mu (1-\phi) J^l\right) dV \\
&= \int_{{\mathcal{B}^l}_0} \left[\frac{D^l\left(\rho_l e_\mu (1-\phi)\right)}{Dt} + \rho_l e_\mu (1-\phi)\frac{j^l}{J^l}\right] J^l dV \\
&= \int_{\mathcal{B}} \left[\frac{D^l\left(\rho_l e_\mu (1-\phi)\right)}{Dt} + \rho_l e_\mu (1-\phi)\mathrm{div}\boldsymbol{v}^l\right] dv \\
&= \int_{\mathcal{B}_0} \left[\frac{D^l\left(\rho_l e_\mu (1-\phi)\right)}{Dt} + \rho_l e_\mu (1-\phi)\mathrm{div}\boldsymbol{v}^l\right] J dV = 0 \ .
\end{aligned} \tag{C-4}$$

Thus, the local form of the liquid mass balance is given by,

$$\left[\frac{D^l\left(\rho_l e_\mu (1-\phi)\right)}{Dt} + \rho_l e_\mu (1-\phi)\mathrm{div}\boldsymbol{v}^l\right] J = 0 \,, \tag{C-5}$$

where $J > 0$ makes it possible, by also expanding the time derivative, to reduce this to,

$$\frac{\partial}{\partial t}\left(\rho_l e_\mu (1-\phi)\right) + \mathrm{grad}\left(\rho_l e_\mu (1-\phi)\right)\cdot \boldsymbol{v}^l + \rho_l e_\mu (1-\phi)\mathrm{div}\boldsymbol{v}^l = 0 \,. \tag{C-6}$$

A relative velocity, $\boldsymbol{v}^{r,l} = \boldsymbol{v}^l - \boldsymbol{v}$, can be used when formulating a Darcian velocity for the liquid phase, $\boldsymbol{v}^{d,l} = e_\mu (1-\phi)\boldsymbol{v}^{r,l}$. Introducing $\boldsymbol{v}^{r,l}$ in the expression above gives,

$$\begin{aligned}
&\frac{\partial}{\partial t}\left(\rho_l e_\mu (1-\phi)\right) + \mathrm{grad}\left(\rho_l e_\mu (1-\phi)\right)\cdot (\boldsymbol{v} + \boldsymbol{v}^{r,l}) + \rho_l e_\mu (1-\phi)\mathrm{div}(\boldsymbol{v} + \boldsymbol{v}^{r,l}) \\
&\qquad = 0 \,,
\end{aligned} \tag{C-7}$$

which by introducing the material time derivative gives,

$$\overline{\rho_l e_\mu \dot{(1-\phi)}} + \mathrm{div}(\rho_l \boldsymbol{v}^{d,l}) + \rho_l e_\mu (1-\phi)\mathrm{div}\boldsymbol{v} = 0\,. \tag{C-8}$$

If expanding the time derivative, we see that,

$$\overline{\rho_l e_\mu \dot{(1-\phi)}} = \dot{\rho}_l e_\mu (1-\phi) + \rho_l \dot{e}_\mu (1-\phi) - \rho_l e_\mu (1-\phi)\mathrm{div}\boldsymbol{v}\,, \tag{C-9}$$

which on insertion gives,

$$\dot{\rho}_l e_\mu (1-\phi) + \rho_l \dot{e}_\mu (1-\phi) + \mathrm{div}(\rho_l \boldsymbol{v}^{d,l}) = 0\,, \tag{C-10}$$

where a source term $f_l^{\,w}$ can be added to the right-hand side.

Gaseous water

The gaseous water mass per mixture volume can be expressed as,

$$\frac{dm_g{}^w}{dv} = \frac{dm_g{}^w}{dv_g}\frac{dv_g}{dv_s}\frac{dv_s}{dv} = \theta_g{}^w\big(e-e_\mu\big)(1-\phi) \tag{C-11}$$

The total gaseous water mass $\mathcal{M}^g$ is obtained from,

$$\mathcal{M}^g = \int_{\mathcal{B}} \theta_g{}^w\big(e-e_\mu\big)(1-\phi)dv = \int_{\mathcal{B}_0} \theta_g{}^w\big(e-e_\mu\big)(1-\phi)JdV = \int_{\mathcal{B}_0} M_g dV\ . \tag{C-12}$$

Performing the same procedure as for the liquid, but now taking the time derivative with respect to the gas reference configuration, and performing a pull-back to/push-back from this configuration, gives,

$$\begin{aligned}
\frac{D^g\mathcal{M}^g}{Dt} &= \frac{D^g}{Dt}\int_{\mathcal{B}^g{}_0} \theta_g{}^w\big(e-e_\mu\big)(1-\phi)J^g dV \\
&= \int_{\mathcal{B}^g{}_0} \frac{D^g}{Dt}\big(\theta_g{}^w\big(e-e_\mu\big)(1-\phi)J^g\big)dV \\
&= \int_{\mathcal{B}^g{}_0} \Bigg[\frac{D^g\Big(\theta_g{}^w\big(e-e_\mu\big)(1-\phi)\Big)}{Dt} \\
&\quad + \theta_g{}^w\big(e-e_\mu\big)(1-\phi)\frac{\dot{J}^g}{J^g}\Bigg]J^g dV \\
&= \int_{\mathcal{B}} \Bigg[\frac{D^g\Big(\theta_g{}^w\big(e-e_\mu\big)(1-\phi)\Big)}{Dt} \\
&\quad + \theta_g{}^w\big(e-e_\mu\big)(1-\phi)\mathrm{div}\boldsymbol{v}^g\Bigg]dv \\
&= \int_{\mathcal{B}_0} \Bigg[\frac{D^g\Big(\theta_g{}^w\big(e-e_\mu\big)(1-\phi)\Big)}{Dt} \\
&\quad + \theta_g{}^w\big(e-e_\mu\big)(1-\phi)\mathrm{div}\boldsymbol{v}^g\Bigg]JdV = 0\ .
\end{aligned} \tag{C-13}$$

Thus, the local form of the gaseous water mass balance is given by,

$$\Bigg[\frac{D^g\Big(\theta_g{}^w\big(e-e_\mu\big)(1-\phi)\Big)}{Dt} + \theta_g{}^w\big(e-e_\mu\big)(1-\phi)\mathrm{div}\boldsymbol{v}^g\Bigg]J = 0\,, \tag{C-14}$$

where $J > 0$ makes it possible, by also expanding the total time derivative (into a spatial one), to reduce to,

$$\frac{\partial}{\partial t}\left({\theta_g}^w\left(e-e_\mu\right)(1-\phi)\right)+\text{grad}\left({\theta_g}^w\left(e-e_\mu\right)(1-\phi)\right)\cdot\boldsymbol{v}^g + {\theta_g}^w\left(e-e_\mu\right)(1-\phi)\text{div}\boldsymbol{v}^g=0\,. \tag{C-15}$$

Using a relative velocity, $\boldsymbol{v}^{r,g}=\boldsymbol{v}^g-\boldsymbol{v}$, a Darcian velocity for the gaseous phase, $\boldsymbol{v}^{d,g}=\left(e-e_\mu\right)(1-\phi)\boldsymbol{v}^{r,g}$ can be formulated. Using $\boldsymbol{v}^{r,g}$ in the expression above results in,

$$\frac{\partial}{\partial t}\left({\theta_g}^w\left(e-e_\mu\right)(1-\phi)\right)+\text{grad}\left({\theta_g}^w\left(e-e_\mu\right)(1-\phi)\right)\cdot(\boldsymbol{v}+\boldsymbol{v}^{r,g}) + {\theta_g}^w\left(e-e_\mu\right)(1-\phi)\text{div}(\boldsymbol{v}+\boldsymbol{v}^{r,g})=0\,. \tag{C-16}$$

When formulating this using a material time derivative makes it possible to arrive at,

$$\dot{\overline{{\theta_g}^w\left(e-e_\mu\right)(1-\phi)}}+\text{div}\left({\theta_g}^w\boldsymbol{v}^{d,g}\right)+{\theta_g}^w\left(e-e_\mu\right)(1-\phi)\text{div}\boldsymbol{v}=0\,, \tag{C-17}$$

and expanding the time derivative,

$$\begin{aligned}\dot{\overline{{\theta_g}^w\left(e-e_\mu\right)(1-\phi)}} &= \dot{\theta}_g{}^w\left(e-e_\mu\right)(1-\phi)+{\theta_g}^w\dot{e}(1-\phi)-{\theta_g}^w\dot{e}_\mu(1-\phi)\\ &\quad-{\theta_g}^w\left(e-e_\mu\right)(1-\phi)\text{div}\boldsymbol{v}\,,\end{aligned} \tag{C-18}$$

gives on insertion,

$$\dot{\theta}_g{}^w\left(e-e_\mu\right)(1-\phi)+{\theta_g}^w\dot{e}(1-\phi)-{\theta_g}^w\dot{e}_\mu(1-\phi)+\text{div}\left({\theta_g}^w\boldsymbol{v}^{d,g}\right)=0\,, \tag{C-19}$$

where a source term ${f_g}^w$could be added to the right-hand side.

Appendix D: Spherical/deviatoric-split

For some cases it is beneficial to study the spherical and deviatoric part of the stress apart. To obtain such a formulation, we start with the stress relation of the model which can be written,

$$-\boldsymbol{\sigma} = \alpha(\Psi_M \mathbf{1} + \Psi_\Delta \boldsymbol{f} - s\mathbf{1})\,. \tag{D-1}$$

Stress and path variables can be divided into spherical and deviatoric parts,

$$\boldsymbol{\sigma} = \frac{1}{3}\mathrm{tr}\boldsymbol{\sigma}\,\mathbf{1} + \boldsymbol{s} = -p\mathbf{1} + \boldsymbol{s}\,, \tag{D-2}$$

$$\boldsymbol{f} = \frac{1}{3}\mathrm{tr}\boldsymbol{f}\,\mathbf{1} + \boldsymbol{f}^{dev} = f_p\,\mathbf{1} + \boldsymbol{f}^{dev}\,. \tag{D-3}$$

Von Mises stress q and a similar invariant for the path variable f_q can be formed using the deviatoric part of the tensors,

$$(q)^2 = \frac{3}{2}\boldsymbol{s}\cdot\boldsymbol{s} \quad \text{and} \quad {f_q}^2 = \frac{3}{2}\boldsymbol{f}^{dev}\cdot\boldsymbol{f}^{dev}\,. \tag{D-4}$$

We may now use the above to arrive at a formulation of the stress relation which are split in spherical and deviatoric parts,

$$-(-p\mathbf{1} + \boldsymbol{s}) = \alpha\Psi_M\mathbf{1} + \alpha\Psi_\Delta\left(f_p\,\mathbf{1} + \boldsymbol{f}^{dev}\right) - \alpha s\mathbf{1}\,, \tag{D-5}$$

which can be written separately,

$$p = \alpha\Psi_M + \alpha\Psi_\Delta f_p - \alpha s \quad \text{and} \quad -\boldsymbol{s} = \alpha\Psi_\Delta\boldsymbol{f}^{dev}\,. \tag{D-6}$$

If starting with the second relation above and multiplying each side by itself and 3/2 we have,

$$\frac{3}{2}\boldsymbol{s}\cdot\boldsymbol{s} = (\alpha\Psi_\Delta)^2\frac{3}{2}\boldsymbol{f}^{dev}\cdot\boldsymbol{f}^{dev} \;\Leftrightarrow\; (q)^2 = (\alpha\Psi_\Delta)^2{f_q}^2\,. \tag{D-7}$$

As a side note, expressions of ${f_p}^2$ and ${f_q}^2$ in terms of components of $\boldsymbol{f}$ is given,

$${f_p}^2 = \frac{1}{9}\left({f_{11}}^2 + {f_{22}}^2 + {f_{33}}^2 + 2(f_{11}f_{22} + f_{11}f_{33} + f_{22}f_{33})\right), \tag{D-8}$$

$${f_q}^2 = {f_{11}}^2 + {f_{22}}^2 + {f_{33}}^2 - f_{11}f_{22} - f_{11}f_{33} - f_{22}f_{33} + 3{f_{12}}^2 + 3{f_{13}}^2 + 3{f_{23}}^2\,. \tag{D-9}$$

Appendix E: Stiffness components at shearing and constant suction

We study the formulation,

$$-\boldsymbol{\sigma} = \alpha(\Psi_M \mathbf{1} + \Psi_\Delta \boldsymbol{f} - s\mathbf{1}) \tag{E-1}$$

$$F = R^2 - \left({f_p}^2 + {f_q}^2\right) \tag{E-2}$$

$$\frac{\partial \boldsymbol{f}}{\partial \boldsymbol{\varepsilon}} = \begin{cases} -\boldsymbol{K}\dfrac{F}{R^2} & dF < 0 \\ -\boldsymbol{K} & dF \geq 0 \end{cases} \tag{E-3}$$

under the conditions,

$$\boldsymbol{\sigma} = \sigma_1 \boldsymbol{e}_1 \otimes \boldsymbol{e}_1 + \sigma_3 \boldsymbol{e}_3 \otimes \boldsymbol{e}_3, \sigma_1 = -\sigma_3 = \sigma_{13} = \sigma_{31} \tag{E-4}$$

$$\boldsymbol{\varepsilon} = \varepsilon_1 \boldsymbol{e}_1 \otimes \boldsymbol{e}_1 + \varepsilon_3 \boldsymbol{e}_3 \otimes \boldsymbol{e}_3, \varepsilon_1 = -\varepsilon_3 = \varepsilon_{13} = \varepsilon_{31} \quad (no\ change\ in\ volume) \tag{E-5}$$

$$ds = 0 \tag{E-6}$$

$$dF < 0 \tag{E-7}$$

Thus,

$$d\boldsymbol{f} = -\frac{F}{R^2}\boldsymbol{K}d\boldsymbol{\varepsilon}\,. \tag{E-8}$$

The incremental form of the model then reduces to,

$$-d\boldsymbol{\sigma} = \alpha\Psi_\Delta d\boldsymbol{f} = -\alpha\Psi_\Delta \frac{F}{R^2}\boldsymbol{K}d\boldsymbol{\varepsilon}. \tag{E-9}$$

For the conditions given above, the component in the first principal direction and when rotated as to obtain maximal shearing read,

$$-d\sigma_{11} = -d\sigma_{13} = -\alpha\Psi_\Delta \frac{F}{R^2} K_{1111}\, d\varepsilon_{11} = -\alpha\Psi_\Delta \frac{F}{R^2} K_{1111}\, d\varepsilon_{13} \tag{E-10}$$

$$-d\sigma_{13} = -\alpha\Psi_\Delta \frac{F}{R^2}(K_{1313}d\varepsilon_{13} + K_{1331}d\varepsilon_{31}) = -\alpha\Psi_\Delta \frac{F}{R^2} 2K_{1313}d\varepsilon_{13} \tag{E-11}$$

$$\Rightarrow 2K_{1313} = K_{1111} \tag{E-12}$$

Appendix F: Rate form of the stress relation

The implementation uses an incremental or rate form (both wordings will be used interchangeably in the following) of the constitutive relation for the stress. The total stress is given by:

$$\boldsymbol{\sigma} = \alpha \boldsymbol{\sigma}^I \,, \tag{F-1}$$

which gives

$$\dot{\boldsymbol{\sigma}} = \alpha\, \dot{\boldsymbol{\sigma}}^I + \dot{\alpha}\, \boldsymbol{\sigma}^I \,. \tag{F-2}$$

Thus, when a rate form of the stress is to be formulated, an expression for the rate $\dot{\alpha}$, i.e.,

$$\dot{\alpha} = \frac{\partial \alpha}{\partial e}\dot{e} + \frac{\partial \alpha}{\partial e_\mu}\dot{e}_\mu \,, \tag{F-3}$$

is needed. Since our selected independent variables to solve for are solid displacements (which can be used to form strains) and suction, the expression above is reformulated somewhat,

$$\dot{\alpha} = \frac{\partial \alpha}{\partial e}\dot{e} + \frac{\partial \alpha}{\partial e_\mu}\left(\frac{\partial e_\mu}{\partial e}\dot{e} + \frac{\partial e_\mu}{\partial \mathrm{s}}\dot{\mathrm{s}}\right) = \left(\frac{\partial \alpha}{\partial e} + \frac{\partial \alpha}{\partial e_\mu}\frac{\partial e_\mu}{\partial e}\right)\dot{e} + \frac{\partial \alpha}{\partial e_\mu}\frac{\partial e_\mu}{\partial s}\dot{\mathrm{s}} \,. \tag{F-4}$$

The void ratio increment can be expressed in terms of strain increment,

$$\dot{e} = \frac{\partial e}{\partial \varepsilon_v}\frac{\partial \varepsilon_v}{\partial \boldsymbol{\varepsilon}} \cdot \dot{\boldsymbol{\varepsilon}} = (1+e)\mathbf{1} \cdot \dot{\boldsymbol{\varepsilon}} \tag{F-5}$$

which makes it possible to arrive at:

$$\dot{\alpha} = \left(\frac{\partial \alpha}{\partial e} + \frac{\partial \alpha}{\partial e_\mu}\frac{\partial e_\mu}{\partial e}\right)(1+e)\mathbf{1} \cdot \dot{\boldsymbol{\varepsilon}} + \frac{\partial \alpha}{\partial e_\mu}\frac{\partial e_\mu}{\partial s}\dot{\mathrm{s}} = a^\varepsilon \mathbf{1} \cdot \dot{\boldsymbol{\varepsilon}} + a^s\, \dot{s} \,. \tag{F-6}$$

where,

$$a^\varepsilon = \left(\frac{\partial \alpha}{\partial e} + \frac{\partial \alpha}{\partial e_\mu}\frac{\partial e_\mu}{\partial e}\right)(1+e) \quad \text{and} \quad a^s = \frac{\partial \alpha}{\partial e_\mu}\frac{\partial e_\mu}{\partial s} \,. \tag{F-7}$$

The increment in total stress can now be expressed in terms of increments in saturated clay grain stress, strain and suction,

$$\dot{\boldsymbol{\sigma}} = \alpha\, \dot{\boldsymbol{\sigma}}^I + a^\varepsilon(\boldsymbol{\sigma}^I \otimes \mathbf{1})\dot{\boldsymbol{\varepsilon}} + a^s \boldsymbol{\sigma}^I\, \dot{s} \,. \tag{F-8}$$

We continue with formulating an expression of the rate of the saturated grain stress beginning with,

$$\boldsymbol{\sigma}^I = \tilde{\boldsymbol{\sigma}}^I(\boldsymbol{\varepsilon}, \boldsymbol{f}, s), \tag{F-9}$$

where the path dependent parameter $\boldsymbol{f}$ has been seen as an independent variable. Since

$$\dot{\boldsymbol{f}} = \frac{\partial \boldsymbol{f}}{\partial \boldsymbol{\varepsilon}}\dot{\boldsymbol{\varepsilon}} \,, \tag{F-10}$$

$\boldsymbol{f}$ is really a function of strain. The present format, however, is selected to obtain a more manageable derivation.

So, on taking the ”time” derivative,

$$\dot{\boldsymbol{\sigma}}^I = \frac{\partial \boldsymbol{\sigma}^I}{\partial \boldsymbol{\varepsilon}}\dot{\boldsymbol{\varepsilon}} + \frac{\partial \boldsymbol{\sigma}^I}{\partial \boldsymbol{f}}\dot{\boldsymbol{f}} + \frac{\partial \boldsymbol{\sigma}^I}{\partial s}\dot{s} \,, \tag{F-11}$$

where,

$$\frac{\partial \boldsymbol{\sigma}^I}{\partial \boldsymbol{\varepsilon}} = \frac{\partial \boldsymbol{\sigma}^I}{\partial \boldsymbol{\psi}}\frac{\partial \boldsymbol{\psi}}{\partial \boldsymbol{\varepsilon}} \quad , \quad \frac{\partial \boldsymbol{\sigma}^I}{\partial \boldsymbol{f}} = \frac{\partial \boldsymbol{\sigma}^I}{\partial \boldsymbol{\psi}}\frac{\partial \boldsymbol{\psi}}{\partial \boldsymbol{f}} \quad \text{and} \quad \frac{\partial \boldsymbol{\sigma}^I}{\partial s} = \frac{\partial \boldsymbol{\sigma}^I}{\partial \boldsymbol{\psi}}\frac{\partial \boldsymbol{\psi}}{\partial s} + \mathbf{1} \,. \tag{F-12}$$

The first derivative, common for all three terms above, is given by,

$$\frac{\partial \boldsymbol{\sigma}^I}{\partial \boldsymbol{\psi}} = -\mathbb{I}, \tag{F-13}$$

where $\mathbb{I}$ denotes the fourth order unit tensor with components $(\mathbb{I})_{ijkl} = \delta_{ik}\delta_{jl}$.

$$\frac{\partial \boldsymbol{\psi}}{\partial \boldsymbol{\varepsilon}} = \frac{\partial \boldsymbol{\psi}}{\partial e_\mu}\frac{\partial e_\mu}{\partial e} \otimes \frac{\partial e}{\partial \varepsilon_v}\frac{\partial \varepsilon_v}{\partial \boldsymbol{\varepsilon}}, \tag{F-14}$$

$$\frac{\partial \boldsymbol{\psi}}{\partial e_\mu} = \frac{\partial \psi_M}{\partial e_\mu}\mathbf{1} + \frac{\partial \psi_\Delta}{\partial e_\mu}\boldsymbol{f} \tag{F-15}$$

$$\frac{\partial e}{\partial \varepsilon_v} = 1 + e \tag{F-16}$$

$$\frac{\partial \varepsilon_v}{\partial \boldsymbol{\varepsilon}} = \mathbf{1} \tag{F-17}$$

$$\frac{\partial \boldsymbol{\psi}}{\partial \boldsymbol{\varepsilon}} = (1+e)\frac{\partial e_\mu}{\partial e}\left(\frac{\partial \psi_M}{\partial e_\mu}\mathbf{1} + \frac{\partial \psi_\Delta}{\partial e_\mu}\boldsymbol{f}\right) \otimes \mathbf{1} \tag{F-18}$$

(F-19)

Thus,

$$\frac{\partial \boldsymbol{\sigma}^I}{\partial \boldsymbol{\varepsilon}} = -\frac{\partial \boldsymbol{\psi}}{\partial \boldsymbol{\varepsilon}} = -(1+e)\frac{\partial e_\mu}{\partial e}\left(\frac{\partial \psi_M}{\partial e_\mu}\mathbf{1} + \frac{\partial \psi_\Delta}{\partial e_\mu}\boldsymbol{f}\right) \otimes \mathbf{1} \tag{F-20}$$

and using index notation,

$$\frac{\partial {\sigma_{ij}}^I}{\partial \varepsilon_{kl}} = -\frac{\partial \psi_{ij}}{\partial \varepsilon_{kl}} = -(1+e)\frac{\partial e_\mu}{\partial e}\left(\frac{\partial \psi_M}{\partial e_\mu}\delta_{ij} + \frac{\partial \psi_\Delta}{\partial e_\mu}f_{ij}\right)\delta_{kl} \tag{F-21}$$

We have that,

$$\frac{\partial \boldsymbol{\psi}}{\partial \boldsymbol{f}} = \psi_\Delta \mathbb{I}\,, \tag{F-22}$$

which gives,

$$\frac{\partial \boldsymbol{\sigma}^I}{\partial \boldsymbol{f}} = \frac{\partial \boldsymbol{\sigma}^I}{\partial \boldsymbol{\psi}}\frac{\partial \boldsymbol{\psi}}{\partial \boldsymbol{f}} = -\psi_\Delta \mathbb{I}\,. \tag{F-23}$$

Finally,

$$\frac{\partial \boldsymbol{\psi}}{\partial s} = \frac{\partial \boldsymbol{\psi}}{\partial e_\mu}\frac{\partial e_\mu}{\partial s}, \tag{F-24}$$

and using the expression for the clay potential derivative,

$$\frac{\partial \boldsymbol{\psi}}{\partial s} = \frac{\partial e_\mu}{\partial s}\left(\frac{\partial \psi_M}{\partial e_\mu}\mathbf{1} + \frac{\partial \psi_\Delta}{\partial e_\mu}\boldsymbol{f}\right), \tag{F-25}$$

which gives,

$$\frac{\partial \boldsymbol{\sigma}^I}{\partial s} = \frac{\partial \boldsymbol{\sigma}^I}{\partial \boldsymbol{\psi}}\frac{\partial \boldsymbol{\psi}}{\partial s} + \mathbf{1} = -\frac{\partial e_\mu}{\partial s}\left(\frac{\partial \psi_M}{\partial e_\mu}\mathbf{1} + \frac{\partial \psi_\Delta}{\partial e_\mu}\boldsymbol{f}\right) + \mathbf{1}\,. \tag{F-26}$$

Returning to,

$$\dot{\boldsymbol{\sigma}}^I = \frac{\partial \boldsymbol{\sigma}^I}{\partial \boldsymbol{\varepsilon}}\dot{\boldsymbol{\varepsilon}} + \frac{\partial \boldsymbol{\sigma}^I}{\partial \boldsymbol{f}}\dot{\boldsymbol{f}} + \frac{\partial \boldsymbol{\sigma}^I}{\partial s}\dot{s}\,, \tag{F-27}$$

and using all the above give,

$$\dot{\boldsymbol{\sigma}}^I = \left[-(1+e)\frac{\partial e_\mu}{\partial e}\left(\frac{\partial \psi_M}{\partial e_\mu}\mathbf{1} + \frac{\partial \psi_\Delta}{\partial e_\mu}\boldsymbol{f}\right) \otimes \mathbf{1} - \psi_\Delta \frac{\partial \boldsymbol{f}}{\partial \boldsymbol{\varepsilon}}\right]\dot{\boldsymbol{\varepsilon}} + \left[\mathbf{1} - \frac{\partial e_\mu}{\partial s}\left(\frac{\partial \psi_M}{\partial e_\mu}\mathbf{1} + \frac{\partial \psi_\Delta}{\partial e_\mu}\boldsymbol{f}\right)\right]\dot{s}\,, \tag{F-28}$$

and if introducing (defining) $\mathbb{C}^I$ and $\mathbb{d}^I$ as,

$$\mathbb{C}^I = -(1+e)\frac{\partial e_\mu}{\partial e}\left(\frac{\partial \psi_M}{\partial e_\mu}\mathbf{1} + \frac{\partial \psi_\Delta}{\partial e_\mu}\boldsymbol{f}\right) \otimes \mathbf{1} - \psi_\Delta \frac{\partial \boldsymbol{f}}{\partial \boldsymbol{\varepsilon}} \tag{F-29}$$

$$\mathbb{d}^I = \mathbf{1} - \frac{\partial e_\mu}{\partial s}\left(\frac{\partial \psi_M}{\partial e_\mu}\mathbf{1} + \frac{\partial \psi_\Delta}{\partial e_\mu}\boldsymbol{f}\right) \tag{F-30}$$

we get,

$$\dot{\boldsymbol{\sigma}}^I = \mathbb{C}^I\dot{\boldsymbol{\varepsilon}} + \mathbb{d}^I\dot{s}. \tag{F-31}$$

Using index notation,

$$\dot{\sigma}^I{}_{ij} = C^I{}_{ijkl}\dot{\varepsilon}_{kl} + d^I{}_{ij}\dot{s}\,. \tag{F-32}$$

where,

$$C^I{}_{ijkl} = -(1+e)\frac{\partial e_\mu}{\partial e}\left(\frac{\partial \psi_M}{\partial e_\mu}\delta_{ij} + \frac{\partial \psi_\Delta}{\partial e_\mu}f_{ij}\right)\delta_{kl} - \psi_\Delta\frac{\partial f_{ij}}{\partial \varepsilon_{kl}} \tag{F-33}$$

$$d^I{}_{ij} = \delta_{ij} - \frac{\partial e_\mu}{\partial s}\left(\frac{\partial \psi_M}{\partial e_\mu}\delta_{ij} + \frac{\partial \psi_\Delta}{\partial e_\mu}f_{ij}\right) \tag{F-34}$$

The increment in total stress can now be expressed in terms of increments in strain and suction,

$$\dot{\boldsymbol{\sigma}} = [\alpha\,\mathbb{C}^I + a^\varepsilon\boldsymbol{\sigma}^I \otimes \mathbf{1}]\dot{\boldsymbol{\varepsilon}} + [\alpha\,\mathbb{d}^I + a^s\boldsymbol{\sigma}^I]\,\dot{s} = \mathbb{C}\,\dot{\boldsymbol{\varepsilon}} + \mathbb{d}\,\dot{s}\,, \tag{F-35}$$

where,

$$\mathbb{C} = \alpha\,\mathbb{C}^I + a^\varepsilon\boldsymbol{\sigma}^I \otimes \mathbf{1} \tag{F-36}$$

$$\mathbb{d} = \alpha\,\mathbb{d}^I + a^s\boldsymbol{\sigma}^I\,. \tag{F-37}$$

On index notation,

$$\dot{\sigma}_{ij} = \left[\alpha C^I{}_{ijkl} + a^\varepsilon\sigma^I{}_{ij}\delta_{kl}\right]\dot{\varepsilon}_{kl} + \left[\alpha d^I{}_{ij} + a^s\sigma^I{}_{ij}\right]\dot{s} = C_{ijkl}\dot{\varepsilon}_{kl} + d_{ij}\dot{s}\,, \tag{F-38}$$

where,

$$C_{ijkl} = \alpha C^I{}_{ijkl} + a^\varepsilon\sigma^I{}_{ij}\delta_{kl} \tag{F-39}$$

$$d_{ij} = \alpha d^I{}_{ij} + a^s\sigma^I{}_{ij}\,. \tag{F-40}$$

Appendix G: Strain-driven formulation of the limiting condition of $\boldsymbol{f}$

An alternative, strain-driven, expression for the limiting condition of $\boldsymbol{f}$ is here derived. The strain-driven format can be used in an expression of the evolution relation for $\boldsymbol{f}$ suitable for implementation in Comsol in that it does not require additional state variables.

The increment of the limiting condition becomes,

$$dF = -2\left(f_p df_p + f_q df_q\right). \tag{G-1}$$

The increment can be expressed further using,

$$df_p = \frac{1}{3}\mathrm{tr}(d\boldsymbol{f}) = \frac{1}{3}\mathbf{1}\cdot d\boldsymbol{f} \tag{G-2}$$

$$f_q{}^2 = \frac{3}{2}\left(\boldsymbol{f} - f_p\,\mathbf{1}\right)\cdot\left(\boldsymbol{f} - f_p\,\mathbf{1}\right) = \frac{3}{2}\left(\boldsymbol{f}\cdot\boldsymbol{f} - 3f_p{}^2\right) \tag{G-3}$$

$$2f_q df_q = \frac{3}{2}\left(2\boldsymbol{f}\cdot d\boldsymbol{f} - 6f_p df_p\right) = 3\left(\boldsymbol{f} - f_p\mathbf{1}\right)\cdot d\boldsymbol{f} \tag{G-4}$$

$$dF = -2f_p df_p - 2f_q df_q = \left(-2f_p\frac{1}{3}\mathbf{1} - 3\left(\boldsymbol{f} - f_p\mathbf{1}\right)\right)\cdot d\boldsymbol{f} = \left(\frac{7}{3}f_p\,\mathbf{1} - 3\boldsymbol{f}\right)\cdot d\boldsymbol{f} \tag{G-5}$$

The evolution equation of the path dependent variable can be expressed as,

$$\text{if } \left[\left(\frac{7}{3}f_p\,\mathbf{1} - 3\boldsymbol{f}\right)\cdot -\boldsymbol{K}d\boldsymbol{\varepsilon} \geq 0\right] \text{ then } \frac{\partial\boldsymbol{f}}{\partial\boldsymbol{\varepsilon}} = -\boldsymbol{K}\,, \qquad \text{else } \frac{\partial\boldsymbol{f}}{\partial\boldsymbol{\varepsilon}} = -\frac{F}{R^2}\boldsymbol{K}\,. \tag{G-6}$$